

# El Agente Estructural: An Artificially Intelligent Molecular Editor

Changhyeok Choi<sup>1,6,†</sup>, Yunheng Zou<sup>2,6,†</sup>, Marcel Müller<sup>1,6</sup>, Han Hao<sup>5</sup>, Yeonghun Kang<sup>1,6</sup>, Juan B. Pérez-Sánchez<sup>1</sup>, Ignacio Gustin<sup>1</sup>, Hanyong Xu<sup>1</sup>, Mohammad Ghazi Vakili<sup>1,2,6</sup>, Chris Crebolder<sup>2,5</sup>, Alán Aspuru-Guzik<sup>1,2,3,4,5,6,7,8,\*</sup>, Varinia Bernales<sup>2,5,\*</sup>

<sup>1</sup>Department of Chemistry, University of Toronto, 80 St. George St., Toronto, ON M5S 3H6, Canada

<sup>2</sup>Department of Computer Science, University of Toronto, 40 St George St., Toronto, ON M5S 2E4, Canada

<sup>3</sup>Department of Materials Science & Engineering, University of Toronto, 184 College St., Toronto, ON M5S 3E4, Canada

<sup>4</sup>Department of Chemical Engineering & Applied Chemistry, University of Toronto, 200 College St., Toronto, ON M5S 3E5, Canada

<sup>5</sup>Acceleration Consortium, 700 University Ave., Toronto, ON M7A 2S4, Canada

<sup>6</sup>Vector Institute for Artificial Intelligence, W1140-108 College St., Schwartz Reisman Innovation Campus, Toronto, ON M5G 0C6, Canada

<sup>7</sup>Canadian Institute for Advanced Research (CIFAR), 661 University Ave., Toronto, ON M5G 1M1, Canada

<sup>8</sup>NVIDIA, 431 King St W #6th, Toronto, ON M5V 1K4, Canada

<sup>†</sup>Contributed equally to this work.

We present EL AGENTE ESTRUCTURAL, a multimodal, natural-language–driven geometry-generation and manipulation agent for autonomous chemistry and molecular modelling. Unlike molecular generation or editing via generative models, ESTRUCTURAL mimics how human experts directly manipulate molecular systems in three dimensions by integrating a comprehensive set of domain-informed tools and vision-language models. This design enables precise control over atomic or functional group replacements, atomic connectivity, and stereochemistry without the need to rebuild extensive core molecular frameworks. Through a series of representative case studies, we demonstrate that ESTRUCTURAL enables chemically meaningful geometry manipulation across a wide range of real-world scenarios. These include site-selective functionalization, ligand binding, ligand exchange, stereochemically controlled structure construction, isomer interconversion, fragment-level structural analysis, image-guided generation of structures from schematic reaction mechanisms, and mechanism-driven geometry generation and modification. These examples illustrate how multimodal reasoning, when combined with specialized geometry-aware tools, supports interactive and context-aware molecular modelling beyond structure generation. Looking forward, the integration of ESTRUCTURAL into EL AGENTE QUNTUR, an autonomous multi-agent quantum chemistry platform, enhances its capabilities by adding sophisticated tools for the generation and editing of three-dimensional structures.

**Date:** February 5, 2026

**Correspondence:** [alan@aspuru.com](mailto:alan@aspuru.com), and [varinia@bernales.org](mailto:varinia@bernales.org)



Acceleration Consortium

## 1 Introduction

Computational chemistry has become an essential tool for understanding molecular structure, reactivity, and materials properties across chemistry, materials science, and catalysis (1, 2, 3). It is widely used in applications such as high-throughput screening (4, 5), materials and catalyst design (2, 6, 7, 8), and mechanistic studies (9, 10), enabling the rational exploration of chemical space beyond what is experimentally accessible.

Recently, in quantum chemistry, agentic systems that directly perform quantum chemistry calculations represent a significant step toward end-to-end automation. In our previous work, we introduced EL AGENTE Q (11), a multi-agent system designed to autonomously execute quantum chemistry calculations. EL AGENTE Q enables users to specify computational tasks through natural-language dialogue and directly performs structure preparation, input generation, computation execution, automated error recovery, and result interpretation within a unified agentic framework. After our work, approaches for computational quantum chemistry workflows have been explored in systems such as ChemGraph (12), AItomia (13), and DREAMS (14) for solid state calculations. In a simultaneous release to this work, we describe in a preprint the capabilities of EL AGENTE QUNTUR (15), a graduate-level computational chemistry agent.

While these systems aim to minimize human intervention in computational workflows, they continue to face challenges in handling molecular geometry, particularly for complex molecules and their modifications. Since chemical properties, including reactivity, electronic structure, and optical properties, are dictated by three-dimensional molecular arrangements, the ability to reliably construct and manipulate molecular geometries is pivotal to computational chemistry research and to understanding structure-property relationships.

Despite the central role of molecular geometry, existing methods for molecular modelling primarily rely on methods with a weak range of control and flexibility, such as database retrieval, SMILES string to 3D geometry conversion with cheminformatics toolkits such as RDKit (16) or Open Babel (17), or generative model (18, 19, 20, 21). They are highly effective for a wide range of applications, as demonstrated in database construction, high-throughput screening, data-driven chemical discovery, and molecular generative modelling (18, 22, 23).

However, the methods described above impose severe limitations when investigating a chemical problem. First, each approach has intrinsic coverage limits: database retrieval is restricted to geometries that already exist in the database; SMILES is designed to encode rigid, covalently bonded (mostly organic) structures and often fails for essential chemically systems such as adducts, reaction intermediates, transition states, and transition-metal complexes, where bonding cannot be straightforwardly classified as covalently single, double, aromatic, or triple; and generative models are constrained by the distributions and representations present in their training data, as well as lack explainability (24).

More fundamentally, these approaches share a common weakness: limited controllability. In many investigations, the goal is not merely to obtain a chemically plausible structure, but to construct a specific geometry that reflects an intended motif or mechanistic condition—e.g., a particular binding mode, coordination arrangement, a stereochemical outcome, or a transition-state (TS)-like geometric distortion—and to vary that condition systematically while keeping other aspects fixed. Such intention-to-geometry translation requires geometry-level operations that can enforce and verify distances, bond angles, dihedral angles, and relative fragment orientations. In contrast, database retrieval and SMILES-based reconstruction offer limited means to specify and enforce these geometric conditions, and distribution-driven generation does not guarantee the selective, composable control required for mechanistic and design investigations.

Conventionally, computational chemists have routinely used three-dimensional molecular editors, such as Avogadro (25), GaussView (26), IQmol (27), Molden (28), and Chemcraft (29), which allow for the direct, interactive manipulation of molecular geometries. These software packages provide useful operations for structure editing, including functional group substitution at selected atomic sites and direct control of interatomic distances, bond angles, and dihedral angles. By interactively modifying atomic positions, chemists can selectively edit target regions of a molecule that reflect their intentions. As a result, this geometry-preserving workflow enables the construction of stereochemically specific structures, reactant-bound complexes, and reaction intermediates or TS-like geometries. Allowing them to flexibly investigate complicated cases, such as catalytic reactions, or hypothesize on chemistry pathways following their reasoning. However, this

process is reasoning-heavy and manual, limiting autonomy and serving as a bottleneck for highly autonomous agentic systems.

To bridge this gap, we introduce EL AGENTE ESTRUCTURAL, an agent for comprehensive molecular structure generation and manipulation via natural-language dialogue. ESTRUCTURAL provides a set of geometry-aware operations and analysis actions that are explicitly designed and implemented based on domain knowledge of how computational chemists analyze, construct, and manipulate three-dimensional molecular structures. Crucially, these operations act directly on atomic indices within **xyz** representations, enabling site-specific manipulation at the level of individual atoms or functional groups. The closest related approach in the literature is SynCraft (30), which introduces a simple set of targeted structural modifications to generated molecules to improve synthesizability, and AtomWorld (31), which includes a 3D geometry editing benchmark for evaluating LLM agents spatial understanding on crystalline materials.

During operation, ESTRUCTURAL reasons about molecular systems geometrically, interpolates geometries both numerically through coordinate analysis and visually by inspecting the resulting geometry. With a wide range of composable actions, we allow simple operations such as functional group substitution, fragment binding, and direct control of interatomic distances, angles, and dihedral angles, to advanced operations including site-selective and symmetry-aware functionalization, fragment-level branch replacement, generation and modification of organometallic structures, TS structures, stereochemical transformations such as enantiomer and *cis/trans* isomer interconversion, and fragment-level structural analysis. ESTRUCTURAL also reasons chemically. In particular, ESTRUCTURAL can interpret chemical schematics—including reaction mechanism diagrams in which intermediates and TS structures are often conveyed visually or are even unknown—and construct the corresponding 3D geometry in an explainable manner.

Through a diverse set of case studies, we demonstrate how ESTRUCTURAL enables on-demand, geometry-consistent manipulation of molecular structures that are difficult to generate or edit using string-based approaches alone. These examples include site-selective functionalization that preserves core geometries, binding of reaction intermediates or ligands to catalytic centers, stereochemically specific construction of transition-metal complexes, geometric operations such as fragment swapping for isomer interconversion, fragment-level structural analysis, and image-guided generation of initial geometries for reaction intermediates and transition states from schematic reaction mechanisms.

At the end of this paper, we discuss future development direction, including the integration of ESTRUCTURAL into EL AGENTE QUINTUR, to enable end-to-end exploration of a substantially broader chemical space in automated quantum chemistry pipelines.

## 2 Methods

### 2.1 System architecture: EL AGENTE ESTRUCTURAL

EL AGENTE ESTRUCTURAL builds upon the cognitive architecture (32) and graphical user interface (GUI) of EL AGENTE Q (11). The system is centred on a single top-level vision-language model (VLM) powered agent, referred to as the **geometry operator agent**, which is responsible for high-level planning, reasoning, and the orchestration of molecular-structure-related tasks (Figure 1).

The **geometry operator** interprets user requests expressed in natural language and decomposes them into a sequence of geometry-aware actions such as structure generation, editing, and structural analysis, by dynamically invoking domain-specific molecular tools and a Python execution environment from a shared tool space. All agents, including the LLM model and tools used in ESTRUCTURAL, are summarized in Table S1.

When reaction information is communicated visually, such as reaction mechanisms communicated through schematic diagrams, the **geometry operator** extracts structural and mechanistic cues from images and returns a structured description of the reaction pathway and geometric information of reaction intermediates, which the **geometry operator** then uses to guide subsequent structure generation and editing steps.

Beyond such diagrammatic inputs, ESTRUCTURAL also supports visual inspection of molecular structures by rendering three-dimensional **xyz** geometries into images at the selected angle and zooming level, allowing the **geometry operator** to verify and reason about spatial arrangements and identify specific atomic indices or

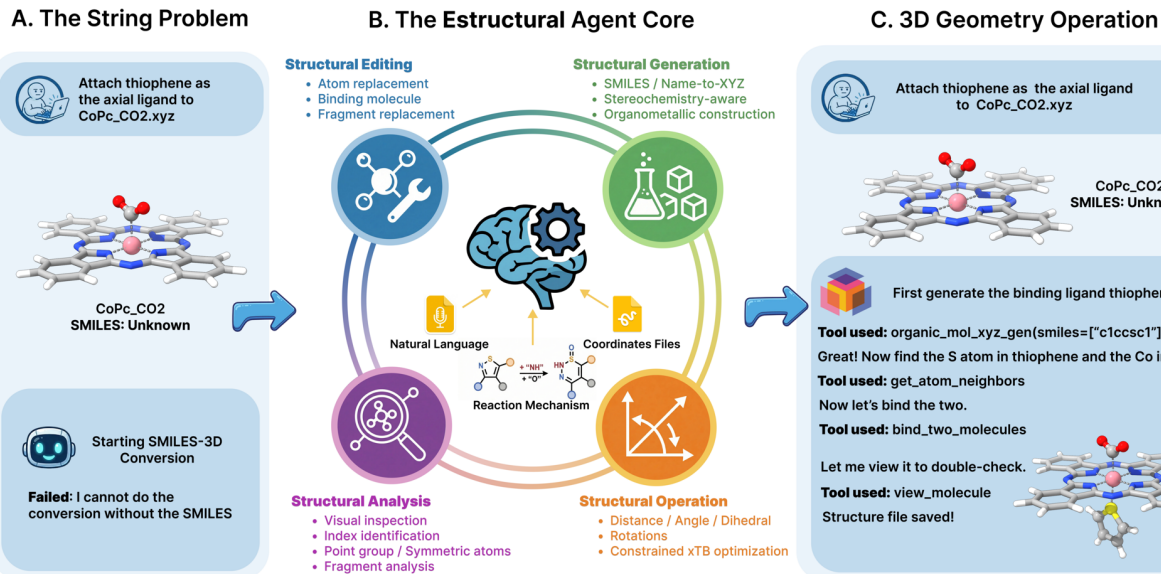


**Figure 1** Schematic overview of the ESTRUCTURAL architecture and workflow. ESTRUCTURAL supports natural-language prompts, coordinate files, and reaction schematics as inputs, and manipulates molecular systems through four action categories: structural editing, structural generation, structural analysis, and geometric operations. The example illustrates attachment of a thiophene ligand to an organometallic complex: ESTRUCTURAL generates the ligand, identifies binding atoms, performs the coordination step, and validates the resulting structure. Atom color codes: pink, Co; yellow, S; red, O; blue, N; gray, C; white, H.

subgroups in the molecule, when needed. This architecture enables flexible coordination between language-based reasoning, visual interpretation, and structure manipulation. To reduce costs and avoid contamination of the LLM and VLM context from prior viewpoints, we employ an image-pruning context management strategy that removes prior molecular system views from memory upon the arrival of new views. This mechanism mimics how humans visually observe only the current snapshot of a scene. This approach saves a significant number of visual tokens as multi-step editing progresses.

## 2.2 The working principle

The key principle—and core innovation—behind ESTRUCTURAL is atomic index-centric geometry operation. This strategy mirrors how chemists manipulate structures in molecular viewers: we click, drag, and adjust angles or torsions, but each interaction ultimately represents a geometric transformation applied to satisfy a spatial intent. The difficulty for an agent is that this workflow relies on continuous, high-frequency hand-eye feedback: humans can "steer" a structure through many micro-adjustments, while an LLM operates in coarse, low-frequency steps. Bridging that gap requires a representation that turns spatial intent into discrete, executable commands.

Atomic indices provide that bridge. An index is an unambiguous handle that links a visually identified atom in a three-dimensional object to its underlying coordinates, allowing the agent to move from qualitative spatial understanding (*closer*, *aligned*, *opened*) to concrete geometry. From these indexed coordinates, the agent can construct geometric primitives—e.g., vectors from two reference points and planes from three reference points—where the reference points are often atom positions but can also be inferred points computed from coordinates (such as bond midpoints, centroids, or fitted ring planes). These primitives then support higher-level relationships such as distances, angles, dihedral angles, and relative orientations. Consequently, most ESTRUCTURAL tools take atomic indices as primary inputs, enabling precise, composable manipulation of molecular geometry without relying on continuous manual dragging. Crucially, these indices must be derived from trusted sources (e.g., a three-dimensional molecular viewer or analysis tools) to ensure that the geometry manipulations are stable and unambiguous.

With atomic indices as stable anchors, ESTRUCTURAL can translate natural-language spatial intent into deterministic, stepwise geometry operations that are repeatable, verifiable, and scalable across complex structures.

## 2.3 Tool design and interface

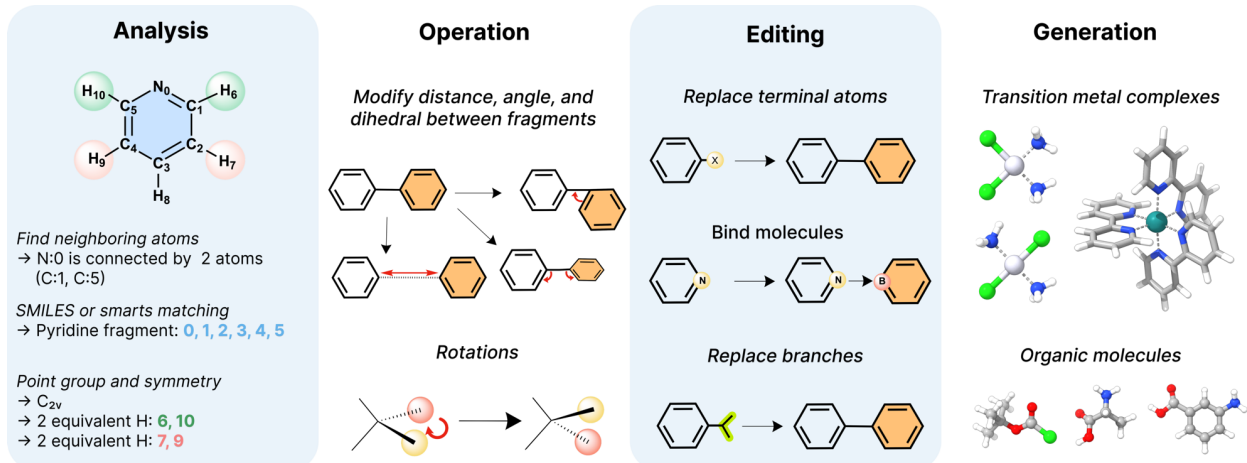


**Figure 2** Overview of the tools integrated into ESTRUCTURAL. The tools are categorized into structural analysis, geometric operation, structure editing, and structure generation, collectively enabling flexible construction, modification, and analysis of molecular geometries. Atom color codes: seashell, Pt; green, Ru; lime green, Cl; blue, N; red, O; gray, C; white, H.

To enable complex molecular manipulations, we introduce a set of specialized tools designed with domain-specific chemical knowledge of how computational chemists construct and manipulate three-dimensional molecular structures in practice (Figure 2). These tools are categorized into four groups based on their functionality: structural analysis, geometric operations, editing, and structure generation, formalizing common viewer-based actions, such as functional group substitution, fragment binding, and direct control of interatomic distances, angles, and dihedral angles, into programmable tools that can be invoked and composed by an LLM agent. The full list of tools is provided in Table S1. The proposed tools are built upon widely adopted open-source Python libraries for molecular and materials modelling, including Atomic Simulation Environment (ASE) (33), RDKit (16), Open Babel (17), spglib (34), and pymatgen (35), which provide reliable representations and operations for atomic structures and chemical graphs. Additionally, the geometry optimization tool uses the Fortran-based `xtb` package (36, 37, 38, 39). Beyond rapid structural optimization, `xtb` is primarily employed to perform constrained geometry optimization, in which selected interatomic distances, angles, and dihedral angles are fixed to certain values. This enables more physically motivated geometric manipulations, which are essential for treating cases such as targeted reaction intermediates and transition-state-like initial structures (see Section 2.3.2 for details).

### 2.3.1 Structural analysis tools

Structural analysis tools are designed to identify atomic indices and structural features within a target molecule that can subsequently be used for structure editing or geometric operations. These tools extract local and global structural information from `xyz` representations, enabling informed and site-selective manipulation of molecular geometries. The arguments of the structural analysis tools, along with representative results, are provided in the Supporting Information Section B.1 and Figure S1.

The `view_xyz` and `zoom_xyz` tools allow the agent to visually observe the molecule in 3D. The 3D view is rendered by PyMol (40) with labelled atomic index and element appear on each atom. This allows the agent to flexibly review the molecular system and spatially identify points of interest or visually verify the resulting geometry after structure editing and geometry operations.

The `python_repl` is a flexible tool that allows the agent to write code to examine the geometry. Through

mostly numpy operations, the agent can easily identify key information, such as the minimum distance between atoms, and verify angles precisely. However, we do not encourage the agent to directly operate on geometries in Python, as empirical results show that Python-based geometry operations can lead to corrupted geometries.

The `get_distance_angle_dihedral` tool is used to calculate interatomic distances, angles, and dihedral angles. Its interface follows the same conventions as the geometric operation tools (Figure S2), allowing measurements to be defined between single atoms or between molecular fragments via centroid dummy atoms.

The `atomic_neighbor_identification` tool takes either an atomic element or a specific atomic index as input and returns all directly connected atoms along with their corresponding indices. This allows efficient characterization of the local coordination environment of a target atom.

The `match_smarts_in_xyz` converts the `xyz` representation into the MOL object format and identifies the atomic indices corresponding to the target fragment. The target fragment can be specified using either SMILES or SMARTS patterns, enabling flexible pattern-based identification of functional groups and substructures.

The `get_connected_subgraph_indices` tool operates using a pair of atomic indices: a starting index and an excluded index. It returns all atomic indices belonging to the branch originating from the starting index, excluding the direction toward the excluded index. This functionality is used internally by both the branch-replacement and geometric-operation tools and enables the identification of complete fragment indices using only a single bond pair.

The `find_pointgroup_equivalent_atoms` determines the molecular point group symmetry and identifies symmetry-equivalent atoms. This capability facilitates automated selection of equivalent sites for symmetric functionalization and coordinated structural modification.

### 2.3.2 Geometric operation tools

Geometric operation tools are designed to directly manipulate molecular geometry by modifying interatomic distances, bond angles, dihedral angles, and fragment orientations through rotation. These operations are applicable not only to individual atoms but also to connected molecular subgroups, enabling coordinated motion of entire fragments rather than isolated atomic displacements.

To modify the interatomic distance between a bonded atom pair  $(i, j)$ , the tool first identifies all atomic indices belonging to the branch extending from atom  $j$ , excluding the direction toward atom  $i$ , following the same branch-identification strategy used in the branch replacement tool. All atoms in the identified branch are then translated collectively to achieve the target distance between atoms  $i$  and  $j$ . This procedure is similarly applied to bond-angle and dihedral-angle modifications, as well as to fragment rotations.

The geometric operation tools support both single atoms and atomic groups as input arguments. When a reference or moving entity is specified as a list of atomic indices rather than a single atom, a centroid dummy atom is temporarily introduced to represent the fragment. Geometric transformations are then defined with respect to distances, angles, or dihedral angles involving either real atoms or these centroid dummy atoms. This design allows the tools to be naturally extended to geometric operations involving metal centers and polydentate ligands.

The rotation tool is conceptually related to dihedral angle manipulation but is particularly useful for generating alternative isomeric configurations. It takes a list of atomic indices defining a base vector, identifies the mutually connected atom shared by these indices, and computes unit vectors from each index to this shared atom. The fragment is then rotated by a specified angle about the resultant vector obtained from the vector sum of the two vectors. This operation enables efficient fragment swapping, facilitating conversion between distinct isomeric forms. Detailed operational mechanisms and arguments are provided in Supporting Information Section B.2 and Figure S2.

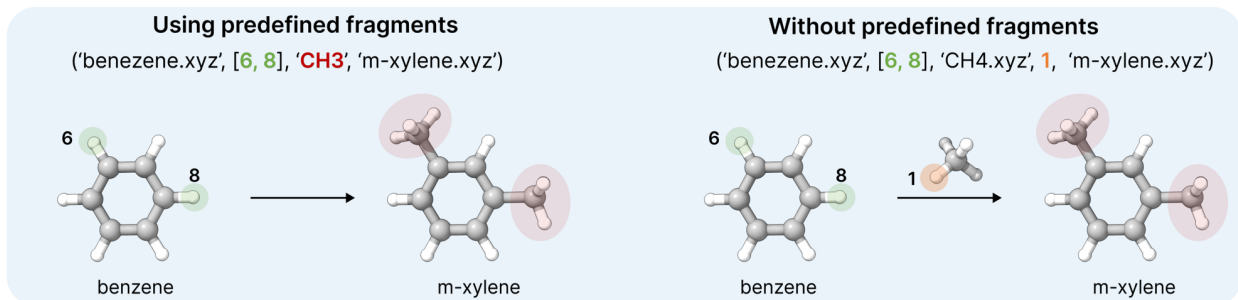
The constrained geometry optimization tool (`constraint_xtb`) employs the semiempirical quantum-mechanical GFN $n$ -xTB methods (36, 37, 39), which are designed for accurate descriptions of geometries, vibrational frequencies, and non-covalent interactions, as well as the related GFN force field from the same family of methods (38). In addition to unconstrained energy minimization with respect to nuclear coordinates for the relaxation of generated structures, harmonic-constraining potentials can be applied to selected distances, bond

angles, and dihedral angles. These additional potentials enable optimizations toward TS-like geometries or the enforcement of specific binding motifs, such as the attachment of molecules to surfaces or the stabilization of metal-organic complexes in predefined configurations. Each constraining potential is defined by the atomic indices it acts on (two for distances, three for angles, and four for dihedral angles) and a force constant expressed in atomic units ( $E_h a_0^{-2}$ ), corresponding to a harmonic potential in Cartesian space. From the perspective of the agent, constrained optimization is exposed as a lightweight Python tool that takes a molecular structure, the relevant atomic indices, and (optionally) the force constant as input, and returns the correspondingly relaxed, constraint-consistent structure. Further details on the technical background are provided in the official `xtb` documentation (see [xtb-docs.readthedocs.io/en/latest/xcontrol.html](https://xtb-docs.readthedocs.io/en/latest/xcontrol.html)).

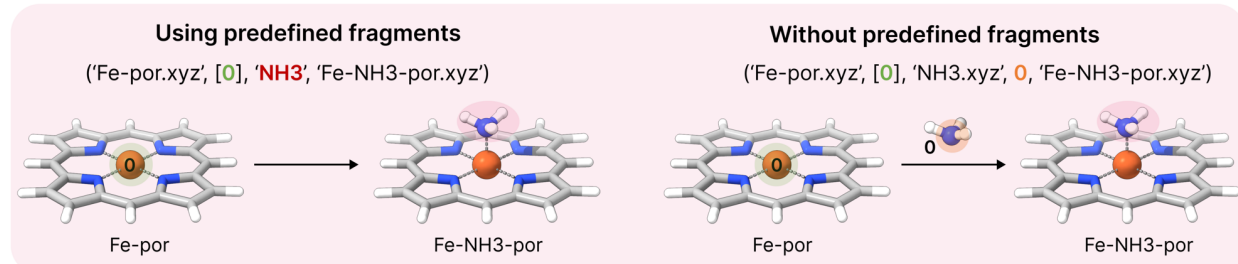
In addition to the operations described above, ESTRUCTURAL provides several auxiliary geometric manipulation tools, including `move_atoms`, `remove_atoms`, and `insert_atom_at_centroid`.

### 2.3.3 Structure editing tools

#### a) Replace terminal atoms



#### b) Bind molecules



#### c) Replace branches

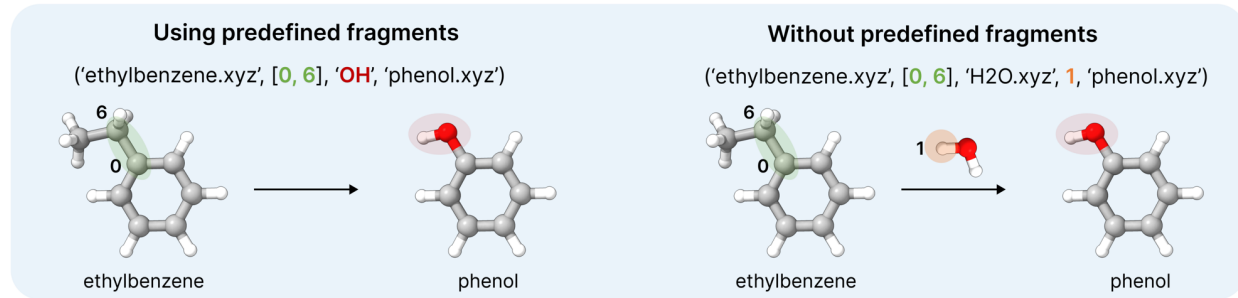


**Figure 3** Schematic illustration of structure editing tools, including (a) terminal atom replacement, (b) molecule binding, and (c) branch replacement. These tools enable functionalization, fragment attachment, and subgroup substitution by modifying selected atomic sites while preserving the rest of the molecular geometry. Representative arguments are shown in each example, including the input `xyz` structure filename, target atomic indices for replacement or binding, fragment specifications, and the name of the newly generated output structure. Atom color codes: dark orange, Fe; red, O; blue, N; gray, C; white, H.

The structure editing tools support three primary operations: replacement of terminal atoms, binding of

molecular fragments to designated atomic sites, and substitution of molecular branches (subgroups) within an `xyz` structure (Figure 3). Across all editing operations, the Cartesian coordinates (or internal coordinates) of atoms outside the replaced region remain unchanged, thereby preserving the original conformation of the molecular core. For all structure editing tools, an additional sanitization step is applied to prevent unphysical atomic overlaps between the core structure and newly attached fragments. If steric clashes are detected at the interface, the attached fragment is iteratively rotated about the newly formed bond until overlaps are resolved, ensuring a physically reasonable initial geometry.

The terminal atom replacement tool is conceptually analogous to functionalization operations in molecular visualization software, in which a functional group is selected and substituted at a chosen terminal atom. This tool takes as input a core `xyz` file to be edited, the atomic indices to replace, and a substituent. To streamline common use cases, we provide a predefined library of frequently used functional groups, allowing fragments to be specified by name alone. If the requested substituent is not available in the library, the agent first generates the corresponding fragment as a standalone `xyz` structure and then attaches it to the specified atomic site, with the connection atom explicitly defined. This design enables highly flexible molecular functionalization, ranging from commonly used substituents to custom-designed fragments. The detailed mechanism and full argument specifications of the terminal atom replacement tool are described in Figure S3.

The molecule binding tool attaches an additional molecular fragment, provided as an `xyz` file, to specified atomic indices within a core molecular structure. Compared to terminal atom replacement, this operation is technically more challenging. While terminal atom replacement can be performed by preserving the internal coordinates of each fragment, fragment binding requires the explicit definition of new inter-fragment bonds with appropriate bond directions. To address this challenge, the tool introduces a pair of dummy atoms, each attached to a designated connection atom in the core structure and the incoming fragment, respectively. These dummy atoms are positioned according to VSEPR-based geometrical considerations, thereby defining both the bonding direction and the initial orientation of the new bond. The binding operation is then carried out by applying the same replacement procedure used in the terminal atom replacement tool, with the dummy atoms serving as temporary connection points. The molecule binding tool supports both predefined fragments from the functional group library and arbitrary `xyz` fragments. Detailed descriptions of the binding mechanism and the positioning strategy for dummy atoms are provided in Figure S4 and S5.

The branch replacement tool substitutes a molecular subgroup (e.g., alkyl chains or ring systems) with an alternative fragment provided as an `xyz` file. The operation is defined using bond pairs specified by atomic index tuples  $(i, j)$  in the core structure, where the branch remains connected to atom  $i$  but originates from atom  $j$ . Given the specified bond pair  $(i, j)$ , the tool first identifies all atomic indices belonging to the branch extending from atom  $j$ , excluding the direction toward atom  $i$ . These branch atoms are then removed from the core structure, with atom  $j$  retained as the replacement point. Subsequently, analogous to the terminal atom replacement procedure, atom  $j$  is replaced with the new branch fragment. This tool is particularly useful for systematic subgroup substitution and ligand exchange reactions. In the context of ligand exchange, the operation can be performed efficiently by specifying the atomic index of the metal center and the coordinating atom within the ligand, enabling rapid modification of coordination environments.

The detailed mechanisms, arguments of the editing tools, and predefined fragments library are provided in Supporting Information Section B.3 and Figure S6.

#### 2.3.4 Structure generation tools

Structure generation tools are designed to construct `xyz` representations of both organic and organometallic molecules. For generating organic molecules, we implement a conversion pipeline that converts SMILES strings to `xyz` coordinates using RDKit (16) and Open Babel (17). Leveraging the pretrained chemical knowledge of the LLM, common names and IUPAC names can be automatically converted into SMILES representations, which are then passed to the generation tool. To improve robustness in cases where the LLM fails to generate a correct SMILES string, ESTRUCTURAL also supports name-based structure retrieval from PubChem database (41) via the `pubchempy`. In such cases, common or systematic names are resolved to canonical SMILES directly from PubChem, providing a reliable fallback mechanism for generating organic molecules.

For organometallic structures, we introduce a builder tool based on predefined coordination symmetry

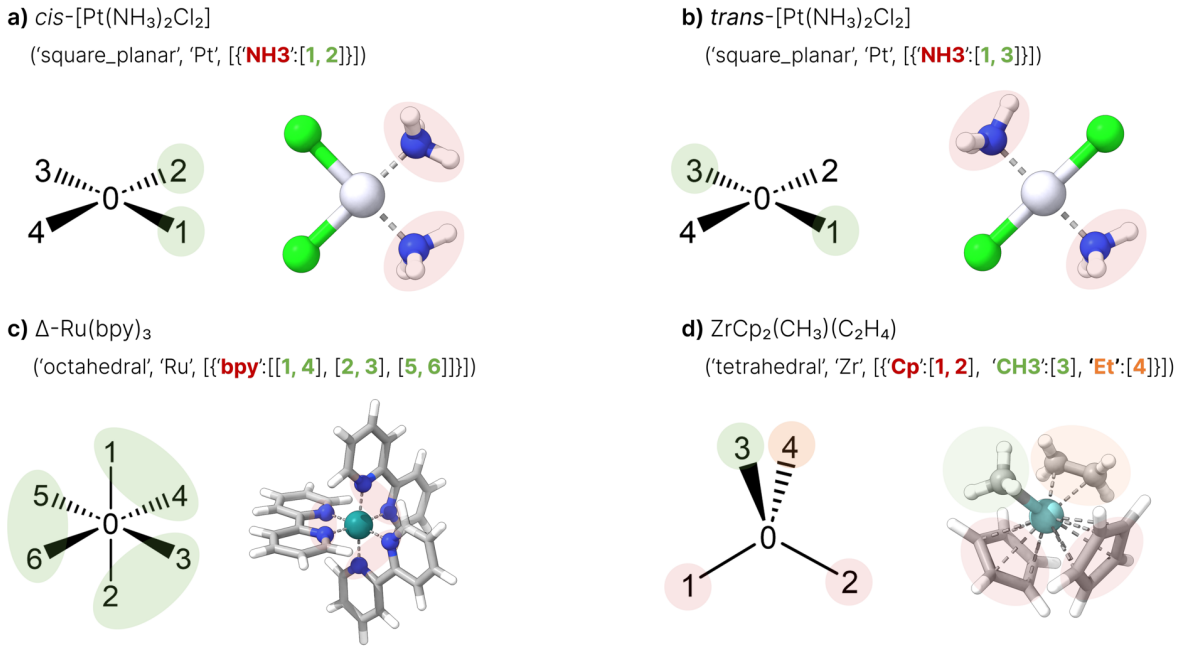


**Figure 4** Overview of structure generation tools for organometallic molecules. Organometallic structures are constructed using predefined coordination–symmetry templates, in which ligands are assigned to annotated atomic indices to generate stereochemically specific geometries. The representative input arguments and the corresponding generated structures for (a) square planar *cis*-[Pt(NH<sub>3</sub>)<sub>2</sub>Cl<sub>2</sub>] and (b) *trans*-[Pt(NH<sub>3</sub>)<sub>2</sub>Cl<sub>2</sub>], (c)  $\Delta$ -Ru(bpy)<sub>3</sub> (bpy = 2,2'-bipyridine), and (d) tetrahedral ZrCp<sub>2</sub>(CH<sub>3</sub>)(C<sub>2</sub>H<sub>4</sub>) (Cp =  $\eta^5$ -cyclopentadienyl). Atom color codes: seashell, Pt; green, Ru; sky blue, Zr; lime green, Cl; blue, N; gray, C; white, H.

templates (Figure 4). This tool requires specification of the central metal, coordination geometry, ligand identities, and their binding positions. Coordination geometries corresponding to coordination numbers from 2 to 6 are predefined. In each coordination template, the central metal atom is assigned a fixed atomic index of 0, while surrounding atoms are initialized as chlorine atoms by default. Each atomic index in the template is annotated with coordination-context information, such as *cis* relationships in square-planar geometries or axial positions in octahedral geometries. After selecting the desired coordination template and replacing the central metal with the target element, ligands are introduced by substituting the corresponding atomic indices with ligand fragments. This procedure enables the generation of stereochemically well-defined organometallic structures. The full set of predefined templates and detailed construction mechanisms is provided in Supporting Information Section B.4 and Figure S7. The builder tool also supports a predefined library of commonly used bidentate and polydentate ligands Figure S8.

For more complex organometallic systems, such as those with high coordination numbers ( $> 6$ ) or multiple polydentate ligands, direct construction from templates may be less practical. In such cases, we provide an alternative tool (`build_predefined_organometallic`) that loads predefined organometallic structures, which can subsequently be modified using the structure editing tools.

### 3 Results

#### 3.1 Vision language model benchmark on spatial understanding

In order for ESTRUCTURAL to perform well on vision-based molecular tasks, we first evaluate a fundamental capability of vision–language models (VLMs): whether they can perceive molecular structures clearly. To quantify this capability, we design a simple benchmark: given a target atom from a molecule, the model must identify its neighboring atoms that are bonded to it. Although this task can be solved easily by computing

interatomic distances and applying empirical bond-length thresholds, the goal here is to assess performance under a vision-only setting.

Accordingly, the benchmarked VLM agent is restricted to using only the `view_molecule` and `zoom_molecule` tools. The system prompt and an example of tool usage is reported in C. We sample 300 molecules from the GeomConf dataset (42) with sizes drawn from a uniform distribution, and benchmark frontier VLMs on this task, including Gemini-3-Pro, Gemini-3-Flash, Claude-Opus-4.5, Claude-4.5-Sonnet, and GPT-5.2-Thinking-High.

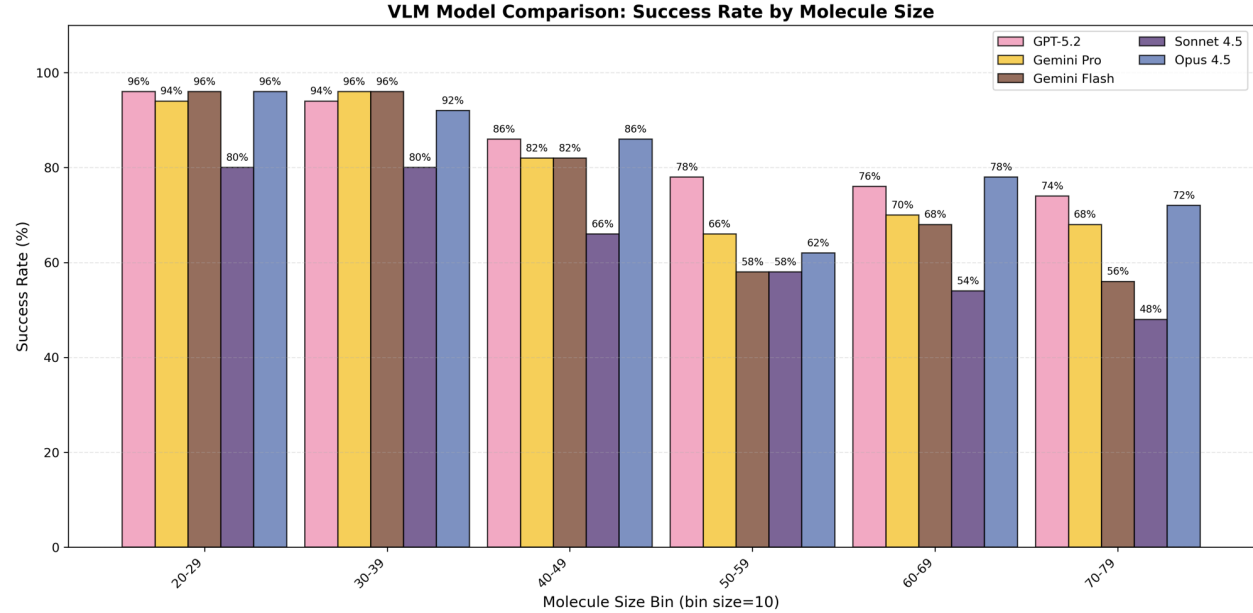


**Figure 5 VLM Benchmark Performance by Molecule Size.** Comparing the success rates of five Vision Language Models (Gemini 3 Pro, Gemini 3 Flash, Sonnet 4.5, Opus 4.5, and GPT 5.2) across varying molecule sizes, measured by the number of atoms. The results illustrate a general trend of decreasing accuracy as molecular complexity increases, with larger systems (60+ atoms) presenting a significant challenge for all tested models.

As shown in Figure 5, all models' performance on this simple task decays significantly as the system size increases, demonstrating rather limited spatial understanding from visual input. In a practical, vision-driven geometric operation process, there must be multi-turn visual inspection, and errors tend to accumulate.

For this reason, the case studies in this work reflect a dynamic strategy in which ESTRUCTURAL selects between explicit structural analysis tools and vision-based inspection depending on the task context. Structural analysis and visual reasoning play complementary roles: connectivity- and index-based analysis provides robustness and scalability for complex, multi-step manipulations, while visual inspection is invoked selectively when it can offer additional intuition or confirmation. This adaptive combination allows the agent to balance reliability with flexibility across diverse molecular systems. We believe that as the model improves over time, the vision understanding bottleneck can be gradually mitigated, as we have already shown in the diagram that Claude Opus 4.5 significantly outperforms Claude Sonnet 4.5. Ether0 (43) and ChemVLM (44) also demonstrated that target training can significantly improve the LLM system's chemistry and vision reasoning capability. Interestingly, Gemini-3-flash didn't underperform Gemini-3-pro on this task, highlighting the potential of smaller VLMs for this application.

### 3.2 Geometry operation case studies

We evaluated ESTRUCTURAL through a series of representative case studies designed to reflect realistic and practically relevant molecular modelling scenarios. These case studies cover a wide range of common tasks, including site-selective functionalization, binding of reactants or ligands to organometallic catalysts, stereochemically selective structure generation, editing of organometallic complexes, interconversion between

stereoisomeric forms, fragment-level structural analysis, and the generation of reaction intermediates and transition-state (TS)-like geometries from a reaction-mechanism schematic provided as a multimodal (image) input.

For each case study, we report the user prompt, the sequence of operations performed by ESTRUCTURAL to address the query, and the resulting `xyz` structures. The case-study figures are presented in a natural language user interface (NLUI) style to visually summarize the interaction between the user and ESTRUCTURAL. In each figure, the user-side speech bubbles show the exact prompt used in the corresponding case study. In contrast, the agent-side speech bubbles show a schematic description of the reasoning steps and tool invocations required to solve each task, as reconstructed by the authors for clarity. The molecular structures shown in the figures correspond either to user-provided input structures or to structures generated by the agent during execution. Newly generated or modified structures are saved by the agent under context-dependent filenames, which are displayed below each structure to indicate the associated `xyz` files; the file extension (`.xyz`) is omitted for readability. All molecular structures are rendered using ChimeraX (45, 46). The structures generated, as well as complete, unedited chat histories for all case studies, including the original agent responses and tool invocations, are available in the <https://github.com/aspru-guzik-group/ElAgenteEstructuralCaseStudies>.

### 3.2.1 Case study 1: Site-selective functionalization

In this case study, we demonstrate site-selective functionalization using ESTRUCTURAL across two representative molecular systems, highlighting both local chemical selectivity and symmetry-guided editing (Figure 6). These tasks require not only identifying appropriate atomic sites but also orchestrating multiple analysis and editing tools.

In the first example, ESTRUCTURAL is tasked with selectively protecting only the primary amines of spermidine, which contains two primary amines and one secondary amine, using tert-butoxycarbonyl (Boc) protecting groups while leaving the secondary amine unchanged. Since neither spermidine nor the Boc group is included in the predefined fragment library, the task requires generating `xyz` structures for both components, identifying the hydrogen atoms to replace on the primary amines, determining the appropriate connection index for the Boc fragment, and performing the corresponding replacement.

Starting from a text prompt, ESTRUCTURAL generates `xyz` structures for spermidine and Boc chloride from SMILES representations. Structural analysis tools are then applied to identify the relevant connection indices in each `xyz` structure. ESTRUCTURAL successfully distinguishes hydrogen atoms bound to primary and secondary amine nitrogen atoms and identifies the chlorine atom in the `Boc_chloride.xyz` file as the appropriate connection site based on local chemical environments. Following identification of the correct replacement sites, a structure editing tool selectively replaces hydrogen atoms on the primary amines with Boc groups, while preserving the remainder of the molecular geometry.

The second example illustrates symmetry-driven site-selective functionalization of a cobalt–porphyrin complex. Symmetrically substituted metal–porphyrin complexes, particularly those functionalized at meso hydrogen positions, have been widely reported in catalytic applications (47). This case study probes ESTRUCTURAL’s ability to perform symmetry-aware functionalization tasks.

Given an existing `xyz` structure, ESTRUCTURAL first performs point group analysis to identify sets of symmetry-equivalent hydrogen atoms. The molecule is classified as belonging to the  $D_{4h}$  point group, revealing two distinct symmetry classes: four equivalent meso hydrogen atoms and eight equivalent  $\beta$  hydrogen atoms. Subsequently, ESTRUCTURAL selectively replaces the four meso hydrogen atoms with phenyl groups, while leaving all other hydrogen atoms unmodified. This enables efficient, symmetry-preserving functionalization without the need to manually specify individual atomic indices. In this case, the phenyl group is available in the predefined fragment library, allowing ESTRUCTURAL to directly use the existing fragment rather than generating an additional `xyz` structure.

These examples demonstrate how ESTRUCTURAL combines structural analysis, on-demand structure generation, and targeted editing to perform reliable site-selective modifications. By flexibly integrating predefined fragments with dynamically generated molecular components, ESTRUCTURAL supports both chemically selective transformations and symmetry-aware functionalization, tasks that would otherwise require manual inspection and intervention by a human expert.

## a) Selective Amine Protection in Spermidine      b) Symmetry-Guided Co-Porphyrin Editing

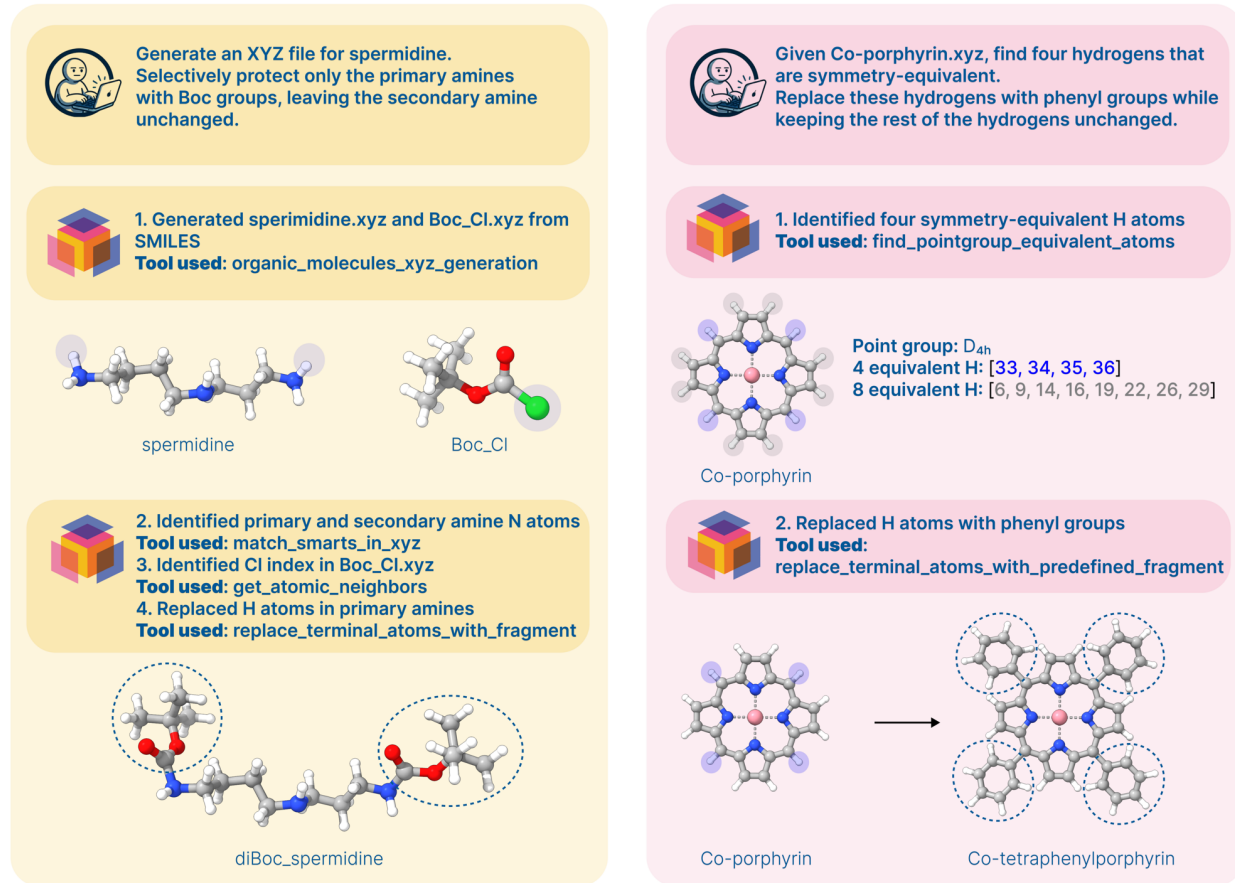


**Figure 6** Representative examples of site-selective functionalization performed by ESTRUCTURAL. (a) Selective protection of primary amines in spermidine, where only terminal amine sites are functionalized with Boc groups while the secondary amine remains unchanged, (b) Symmetry-guided functionalization of a cobalt-porphyrin complex, in which four symmetry-equivalent hydrogen atoms are identified and selectively replaced with phenyl groups while preserving all other hydrogen atoms. The atomic sites selected for replacement and the newly introduced fragments are highlighted for clarity. Atom color codes: pink, Co; lime green, Cl; red, O; blue, N; gray, C; white, H.

### 3.2.2 Case study 2: Binding of reaction intermediates and ligands

In this case study, we evaluate the ability of ESTRUCTURAL to bind reaction intermediates and ligands to a transition-metal catalyst, a common operation in computational catalysis (Figure 7). The target system is a cobalt-phthalocyanine (Co-Pc) complex, which has been widely studied in electrochemical  $\text{CO}_2$  reduction ( $\text{CO}_2\text{RR}$ ) (48, 49, 50, 51) and oxygen reduction reactions (ORR) (52). This case study consists of two sequential user prompts: binding reaction intermediates to the catalyst and subsequently introducing axial ligands, which are known to modulate catalytic activity (53, 54, 55).

In the first step, the user requests binding of key reaction intermediates relevant to electrochemical  $\text{CO}_2$  reduction, hydrogen evolution, and ORR ( $\text{CO}_2$ ,  $\text{COOH}$ ,  $\text{CO}$ ,  $\text{H}$ ,  $\text{OH}$ , and  $\text{H}_2\text{O}$ ) to the cobalt center of the Co-Pc complex. Starting from the provided Co-Pc xyz structure, ESTRUCTURAL employs fragment binding tools to attach each fragment to the cobalt atom, producing a series of Co-Pc structures bound with the corresponding reaction intermediates.

Following completion of the initial binding tasks, a subsequent user query explores the effect of axial ligands. Both the original bare Co-Pc complex and the previously modified Co-Pc structures are taken as inputs. For each structure, an axial ligand (thiophene, pyridine, or chloride) is correctly attached to the cobalt center,

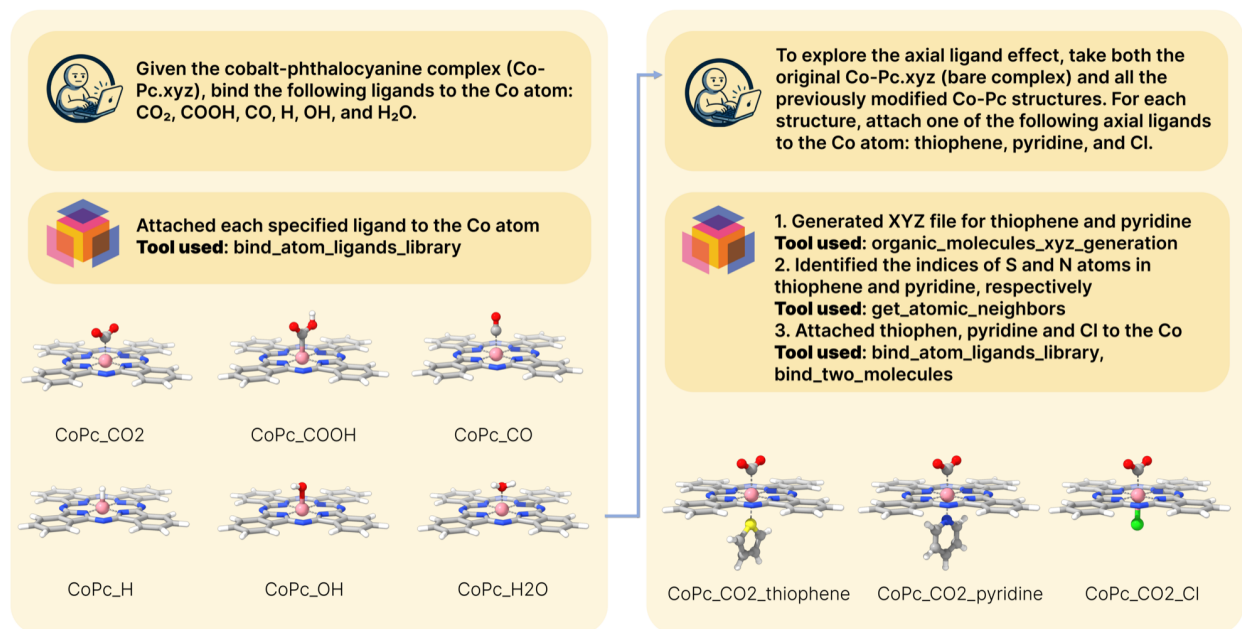


**Figure 7** Binding of reaction intermediates and axial ligands to a cobalt–phthalocyanine (Co-Pc) complex. The generated xyz structures are shown. In this example, sequential prompts are used first to bind reaction intermediates to the cobalt center and, subsequently, to introduce axial ligands. The Co center, together with the bound intermediates (CO<sub>2</sub>, COOH, CO, H, OH, and H<sub>2</sub>O), and axial ligands (thiophene, pyridine, or Cl) are highlighted using a ball-and-stick representation, while the remaining atoms are rendered as sticks for clarity. For axial-ligand–bound structures, only the CO<sub>2</sub>-bound complexes are shown here. The full set of axial-ligand–coordinated structures is provided in the Figure S10. Atom color codes: pink, Co; lime green, Cl; yellow, S; red, O; blue, N; gray, C; white, H.

leading to octahedral coordination. This sequential workflow demonstrates that ESTRUCTURAL can operate on intermediate results, reusing and further modifying previously generated structures without restarting the process.

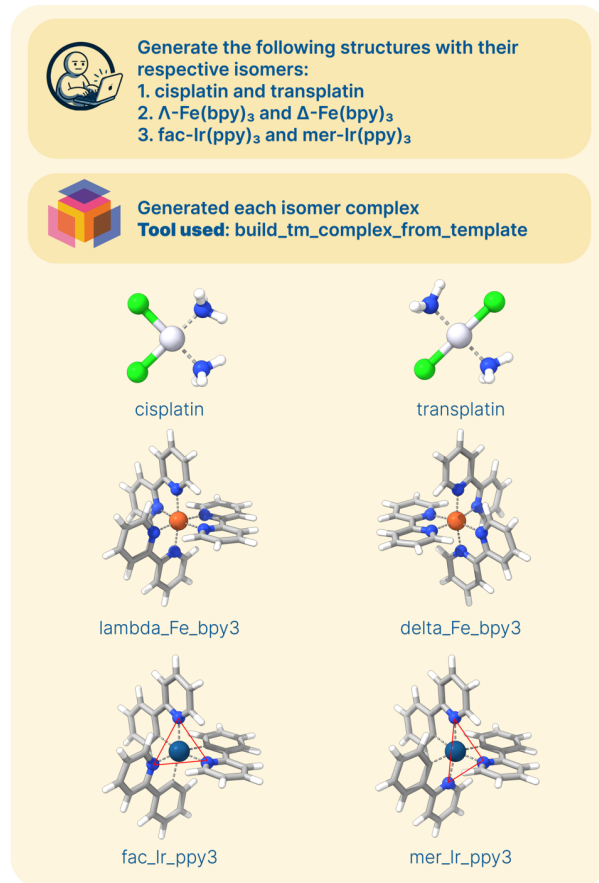
These results highlight the capability of ESTRUCTURAL to perform chemically meaningful fragment binding operations on transition-metal complexes. Importantly, this case study illustrates an interactive workflow in which successive user queries build upon intermediate outputs, enabling iterative refinement of molecular structures. By combining structural analysis, fragment generation, and targeted binding within the interaction paradigm, ESTRUCTURAL enables construction of catalyst–intermediate and catalyst–ligand geometries that are directly relevant to mechanistic and catalytic studies.

### 3.2.3 Case study 3: Organometallic complex construction with stereochemical and ligand variations

In this case study, we demonstrate the ability of ESTRUCTURAL to generate organometallic complexes with specified symmetry, stereochemistry, and ligand coordination (Figure 8). Generating such structures is a non-trivial task, as SMILES-based representations offer limited support for coordination environments, metal–ligand bonding, and stereochemical variants commonly encountered in organometallic chemistry. Even when organometallic structures can be encoded, reliably generating specific stereoisomers, such as *cis/trans*, *fac/mer*, or  $\Delta/\Lambda$  enantiomers, remains challenging within conventional string-based molecular representations. Addressing these limitations is essential for studying structure–property relationships and reactivity trends in coordination chemistry and catalysis.

In this case study, the user requests the generation of multiple stereoisomeric complexes, including cisplatin and transplatin,  $\Delta$ - and  $\Lambda$ -Fe(bpy)<sub>3</sub> (bpy = 2,2'-bipyridine), and *fac*- and *mer*-Ir(ppy)<sub>3</sub> (ppy = 2-phenylpyridine). These systems represent common classes of geometric and chiral isomerism in coordination compounds. By selecting predefined coordination templates and specifying ligand identities and binding positions, ESTRUCTURAL constructs the corresponding xyz structures directly, ensuring the correct relative arrangement of

### a) Selective Isomer Generation



### b) Generation for Zirconocenes

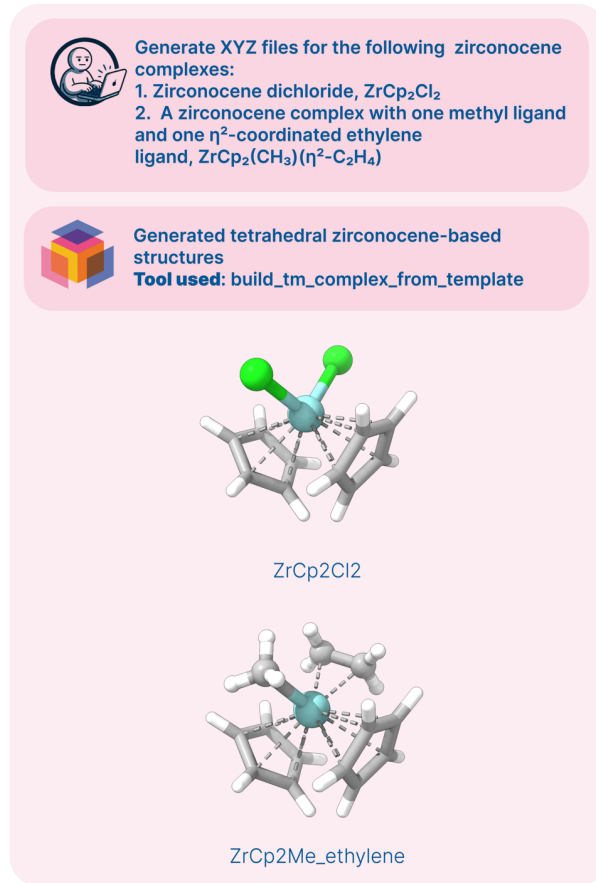


**Figure 8** Generation of organometallic complexes with specified stereochemistry and ligand composition. (a) Generation of stereoisomeric pairs, including cisplatin/transplatin,  $\Lambda$ - and  $\Delta$ -Fe(bpy)<sub>3</sub>, and fac- and mer-Ir(ppy)<sub>3</sub>. For Fe(bpy)<sub>3</sub> and Ir(ppy)<sub>3</sub>, the transition metal centers and the coordinating N atoms that define the stereochemistry are highlighted in ball-and-stick representation, while the remaining atoms are shown as sticks for clarity. For fac- and mer-Ir(ppy)<sub>3</sub>, a red triangle is added to indicate the geometric arrangement of the coordinating N atoms to Ir. (b) Construction of zirconocene-based complexes with varying ligand sets, including ZrCp<sub>2</sub>Cl<sub>2</sub> and ZrCp<sub>2</sub>(CH<sub>3</sub>)( $\eta^2$ -C<sub>2</sub>H<sub>4</sub>)<sup>+</sup>. Cyclopentadienyl (Cp) rings are shown in stick models for clarity. Atom color codes: dark blue, Ir; seashell, Pt; sky blue, Zr; dark orange, Fe; lime green, Cl; red, O; blue, N; gray, C; white, H.

ligands around the metal center.

In addition to stereochemical variants, ligand substitution and coordination mode variations are demonstrated using zirconocene-based complexes. Starting from a tetrahedral coordination template, ESTRUCTURAL generates ZrCp<sub>2</sub>Cl<sub>2</sub> (Cp = cyclopentadienyl) and subsequently constructs a mixed-ligand complex containing one methyl and one  $\eta^2$ -coordinated ethylene ligand, ZrCp<sub>2</sub>(CH<sub>3</sub>)( $\eta^2$ -C<sub>2</sub>H<sub>4</sub>)<sup>+</sup>.

To test whether ESTRUCTURAL can generate organometallic structures through geometric reasoning and operations rather than relying on predefined coordination symmetry templates, we performed an additional case study on the construction of concave and convex CpRu( $\eta^6$ -sumanene)<sup>+</sup> complexes, in which Ru is coordinated by an  $\eta^6$ -sumanene ligand and an  $\eta^5$ -Cp ring (Figure 9).

ESTRUCTURAL first identifies the correct SMILES representation of sumanene using the `look_up_smiles` tool, which maps common names to SMILES strings via the PubChem database, and subsequently generates the corresponding xyz structure. The agent then identifies the carbon atom indices of the central hexagonal ring using a combination of visual inspection and a SMARTS-based pattern matching tool. A Ru atom is inserted at the centroid of the identified hexagonal ring using the geometric operation tool `insert_atom_at_-`

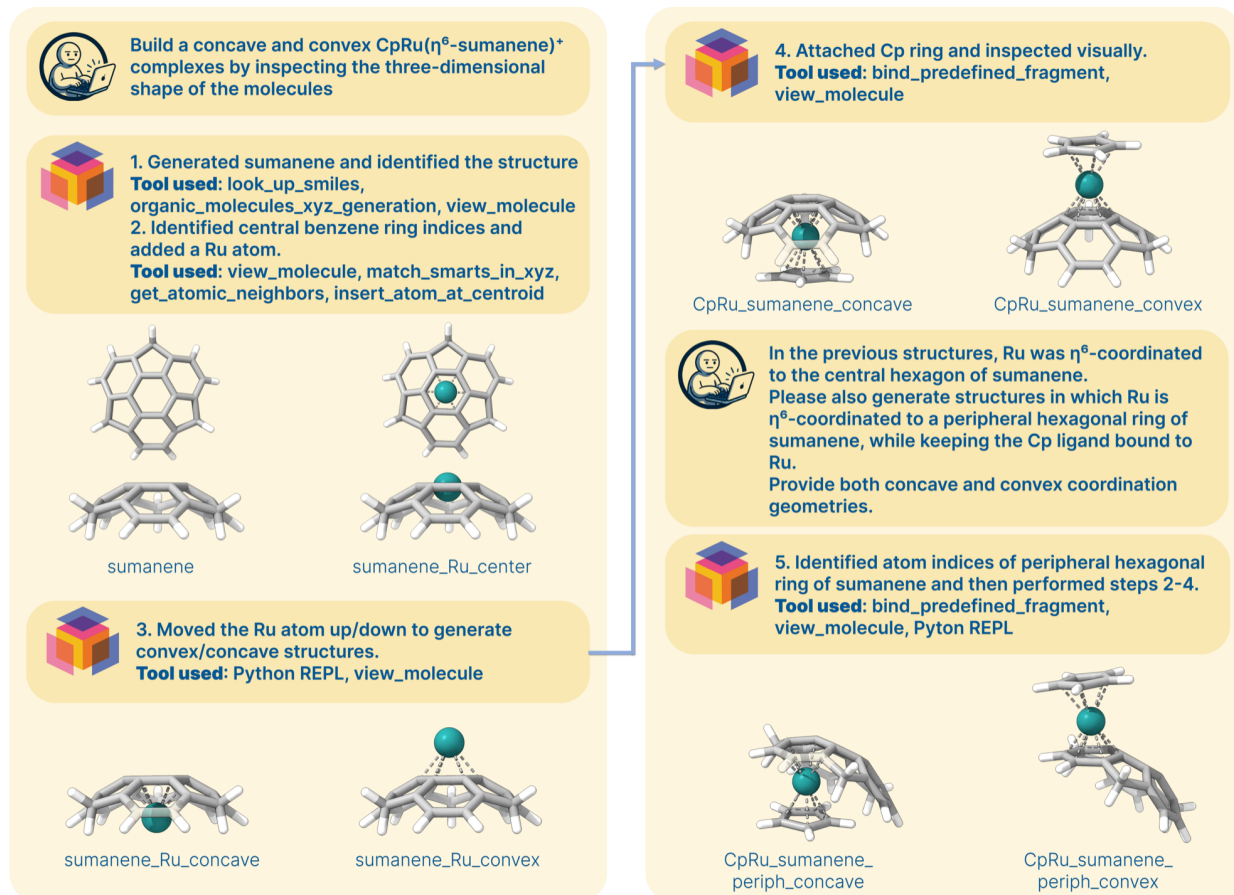


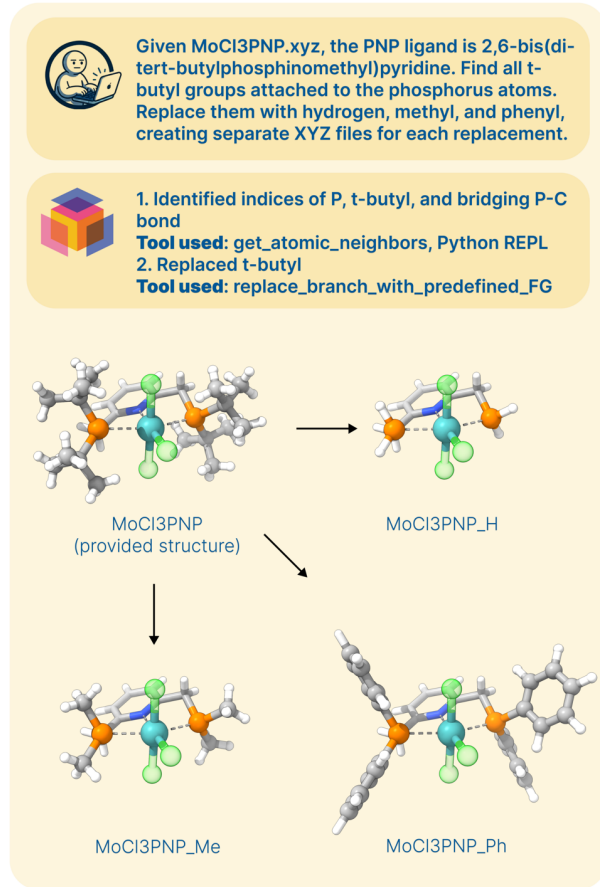
**Figure 9** Stepwise construction of concave and convex  $\text{CpRu}(\eta^6\text{-sumanene})^+$  complexes by ESTRUCTURAL. Initial construction of concave and convex  $\text{CpRu}(\eta^6\text{-sumanene})^+$  complexes with Ru coordinated to the central hexagonal ring of sumanene, and extension of the construction in response to a follow-up prompt, generating concave and convex structures in which Ru is  $\eta^6$ -coordinated to a peripheral hexagonal ring while retaining the Cp ligand. Atom color codes: teal, Ru; gray, C; white, H.

centroid, and its position is displaced along the molecular normal to generate concave and convex coordination geometries, with the displacement direction determined using the Python REPL tool. The resulting  $\text{Ru}(\eta^6\text{-sumanene})$  geometries are visually inspected to confirm the concave or convex configuration, after which the Cp ligand is attached using the predefined fragment binding tool.

Although this procedure successfully generates structures consistent with the initial query, the coordination site was not explicitly specified. In  $\text{CpRu}(\eta^6\text{-sumanene})^+$  complexes, Ru is coordinated to a peripheral hexagonal ring rather than the central ring (56). To address this, a follow-up prompt was issued requesting the construction of  $\text{CpRu}(\eta^6\text{-sumanene})^+$  complexes in which Ru is  $\eta^6$ -coordinated to a peripheral hexagonal ring, for both concave and convex geometries. In response, ESTRUCTURAL correctly identifies the carbon atom indices of a peripheral hexagonal ring, repositions the Ru atom accordingly, and attaches the Cp ligand to generate the desired coordination structures.

An important aspect of this case study is the visual identification of concave and convex coordination geometries. Although such distinctions can, in principle, be described using distances or angles relative to a reference plane, they are often more naturally and robustly recognized through visual inspection of the overall three-dimensional shape. In practice, chemists frequently rely on visual cues to distinguish concave and convex coordination modes, as these features arise from the collective spatial arrangement of many atoms rather than from any single geometric parameter. In this case, ESTRUCTURAL similarly employed visual inspection to confirm whether the  $\text{Ru}(\eta^6\text{-sumanene})^+$  complex adopted a concave or convex configuration following

### a) Substitution of PNP tert-Butyl Groups



### b) Ligand Exchange in Metal Complexes

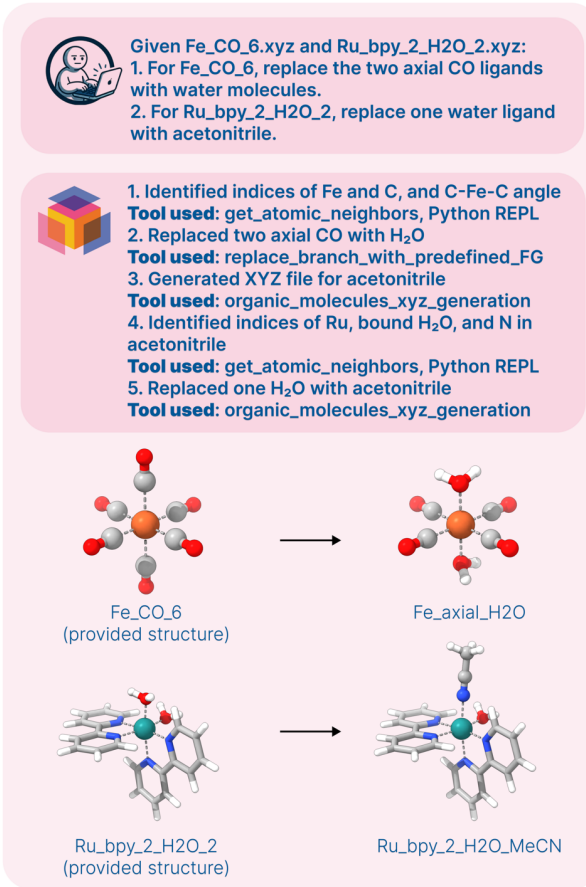


**Figure 10** Fragment-level replacement and ligand exchange in organometallic complexes. (a) Functionalization of a literature-reported MoCl<sub>3</sub>-PNP complex through systematic replacement of tert-butyl groups on a polydentate PNP ligand with hydrogen, methyl, and phenyl substituents. (b) Ligand exchange in transition-metal complexes, including replacement of axial CO ligands with water in an octahedral Fe(CO)<sub>6</sub> and substitution of a coordinated water molecule with acetonitrile in a Ru(bpy)<sub>2</sub>(H<sub>2</sub>O)<sub>2</sub> complex. In all cases, fragment-level replacements are performed while preserving the underlying coordination framework. For the MoCl<sub>3</sub>PNP and Ru(bpy)<sub>2</sub>(H<sub>2</sub>O)<sub>2</sub> complexes, the substituted groups and newly introduced ligands are highlighted using a ball-and-stick representation, while the remaining parts of the molecular framework are rendered as sticks for clarity. Atom color codes: green, Ru; light cyan, Mo; dark orange, Fe; lime green, Cl; orange, P; blue, N; gray, C; white, H.

geometric manipulation. This demonstrates how visual reasoning can effectively complement numerical geometric operations, particularly for global shape features that are difficult to capture using simple distance- or angle-based criteria alone.

More broadly, these results illustrate how ESTRUCTURAL enables on-demand and stereochemically specific construction of organometallic complexes. Notably, ESTRUCTURAL is not restricted to predefined coordination symmetries and can construct valid organometallic structures even when the target coordination environment is not explicitly encoded in the template library. Together with the other case studies presented in this work, this capability provides a practical foundation for generating well-defined isomeric input structures for computational studies without requiring manual assembly or extensive, ad hoc geometric tuning.

#### 3.2.4 Case study 4: Fragment-level replacement in organometallic complexes

In this case study, we demonstrate fragment-level replacement operations in organometallic complexes using ESTRUCTURAL (Figure 10). Constructing organometallic systems from scratch is often challenging,

particularly for complexes featuring polydentate ligands and intricate coordination environments. In such cases, identifying an existing core structure and performing targeted modifications can be a more practical and reliable strategy.

The first example illustrates functionalization of an organometallic complex reported in the literature. The input structure is a  $\text{MoCl}_3$ –PNP complex featuring a tridentate 2,6-bis(di-tert-butylphosphinomethyl)pyridine (PNP) ligand, which has been reported as an efficient catalyst for dinitrogen reduction to ammonia (57). The initial `xyz` structure is taken directly from the corresponding literature source. To investigate the effect of different substituents attached to the phosphorus atoms, constructing entirely new PNP ligands and rebuilding the corresponding metal complexes from scratch would be unnecessarily cumbersome. Instead, a more practical approach is to functionalize the existing Mo–PNP core structure. This scenario motivates the present case study, in which the user requests replacement of the tert-butyl substituents in the PNP ligand of the given Mo–PNP complex.

Starting from the literature-derived  $\text{MoCl}_3$ –PNP structure, ESTRUCTURAL identifies atomic indices of all tert-butyl groups attached to the phosphorus atoms through structural analysis. Using the replacing branches tools, each tert-butyl group is systematically substituted with hydrogen, methyl, and phenyl groups, generating separate `xyz` structures for each modified complex. This example demonstrates how fragment-level editing enables exploration of ligand substituent effects while preserving the original metal coordination environment.

The second example focuses on ligand-exchange reactions, highlighting ESTRUCTURAL’s ability to replace not only terminal atoms but also entire ligand fragments. The user requests ligand exchange operations on two given complexes:  $\text{Fe}(\text{CO})_6$  and  $\text{Ru}(\text{bpy})_2(\text{H}_2\text{O})_2$ . For the  $\text{Fe}(\text{CO})_6$  complex, ESTRUCTURAL first identifies the six carbon atoms coordinated to the Fe center using the `get_atomic_neighbors` tool. It then analyses the C–Fe–C angles between all carbon pairs using a Python-based analysis to determine their relative coordination geometry. Among these, a trans pair is selected based on a C–Fe–C angle larger than  $170^\circ$ , corresponding to the two axial CO ligands. These two axial CO ligands are subsequently replaced with water molecules using the replacing branches tool, while preserving the remaining coordination environment. In a separate  $\text{Ru}(\text{bpy})_2(\text{H}_2\text{O})_2$  complex, one coordinated water ligand is replaced with acetonitrile. Since acetonitrile is not included in the predefined fragment library, ESTRUCTURAL generates its `xyz` structure on demand and subsequently uses it for the ligand exchange operation. This demonstrates that ligand exchange is not limited to predefined fragments and can flexibly accommodate arbitrary ligand species. These transformations are carried out using replacement branch tools and structural analysis tools, enabling selective modification of bound ligands without disrupting the remaining coordination framework.

Overall, this case study demonstrates that ESTRUCTURAL supports fragment-level replacement and ligand exchange operations commonly encountered in organometallic chemistry. By enabling targeted modification of existing coordination complexes, the agent offers a flexible alternative to constructing organometallic structures from scratch, facilitating the efficient exploration of ligand effects and ligand-exchange processes.

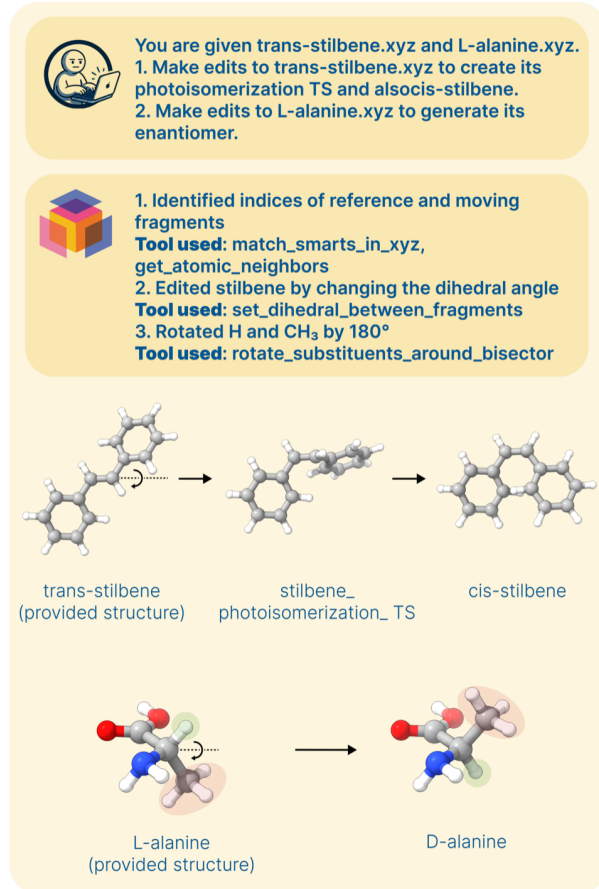
### 3.2.5 Case study 5: Molecular fragment operations and fragment analysis

In this case study, we demonstrate ESTRUCTURAL’s ability to manipulate and identify molecular fragments using geometric operations and structural analysis tools. These capabilities complement structure generation and editing by enabling controlled isomer interconversion and fragment-aware analysis of complex molecular systems (Figure 11).

We consider isomer interconversion in organic molecules, a common task in molecular modeling. Here, we focus on two representative cases: *cis/trans* isomerization of an alkene and enantiomer interconversion of an amino acid (Figure 11a).

Alkene-centered *cis/trans* isomerization is frequently observed in photoexcited states and underlies the function of molecular photoswitches (58, 59). Accordingly, modeling both isomers and intermediate transition-state–like geometries is essential for studying photochemical reaction pathways. Starting from the provided trans-stilbene structure, ESTRUCTURAL identifies the relevant molecular fragments and applies geometric operation tools to systematically modify the dihedral angle between the phenyl groups. By setting the dihedral angle to  $0^\circ$  and  $90^\circ$ , the agent generates the *cis*-stilbene isomer and a TS-like geometry associated with photoisomerization, respectively.

## a) Isomer and Enantiomer Conversion



## b) Molecular Fragment Identification

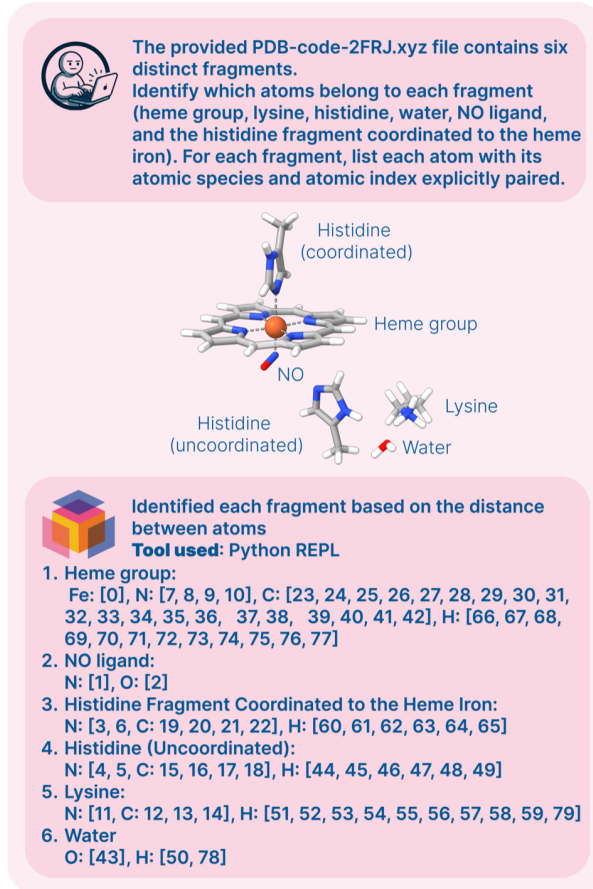


**Figure 11** Molecular fragment operations and fragment analysis enabled by ESTRUCTURAL. (a) Conversion between isomeric forms through geometric operations, including the generation of *cis*-stilbene and a photoisomerization TS-like geometry from *trans*-stilbene, as well as enantiomer generation from L-alanine. (b) Fragment-level structural analysis of a multi-component system derived from a PDB structure, where distinct fragments, including a heme group, coordinated NO, uncoordinated histidine, lysine, and  $\text{H}_2\text{O}$ , are identified, and atom indices are assigned explicitly for each fragment. Atom color codes: dark orange, Fe; red, O; blue, N; gray, C; white, H.

As a case study for enantiomer interconversion, we considered the conversion of the given L-alanine structure to D-alanine. Beginning with L-alanine, ESTRUCTURAL identifies the atomic environment around the stereogenic carbon center and generates the corresponding enantiomer by applying a targeted geometric rotation. Specifically, the hydrogen atom and methyl group bonded to the stereogenic carbon are rotated by  $180^\circ$  around the C–substituent bisector, effectively swapping their relative positions and yielding D-alanine. Such stereochemical conversions are relevant in biomolecular modeling and ligand preparation, where the correct enantiomer is often required.

The second example highlights fragment-level structural analysis for large molecular systems (Figure 11b). For large molecular systems, it is often desirable to freeze redundant fragments during constrained-geometry optimization or to treat them with lower-level methods to reduce computational cost (e.g., QM/MM). To support such workflows, ESTRUCTURAL is tasked with identifying atomic indices in each fragment from a multi-fragment system derived from a PDB structure adapted from an example in the ORCA 6.0 manual (Section 6.3.7) (60, 61). The agent correctly identifies and separates distinct fragments, including the heme group, coordinated and uncoordinated histidine residues, lysine, a nitric oxide ligand, and water molecules, and reports explicit atomic species and index mappings for each fragment.

This case study illustrates how ESTRUCTURAL integrates fragment-level geometric operations with detailed

structural analysis to support isomer control and fragment-aware modelling. These capabilities are particularly valuable for preparing stereochemical-specific input structures and defining fragment constraints in large-scale electronic structure and multiscale simulations.

An additional aspect of this case study highlights the agentic flexibility of ESTRUCTURAL in selecting appropriate analysis strategies. While ESTRUCTURAL employs dedicated structural analysis tools such as `match_smarts_in_xyz` and `get_atomic_neighbors` to identify target indices in other case studies, in this instance, the agent implemented a custom connectivity-based partitioning procedure using a Python execution environment.

To better understand this behaviour, we further queried the agent regarding its choice of analysis strategy. The agent explained that this decision reflects inherent limitations of pattern-based substructure matching in complex metal-organic systems. In the present heme-containing structure, conventional SMARTS-based matching was found to be fragile due to altered bonding geometries and delocalized electronic structures induced by metal coordination, leading to incomplete or inconsistent identification of coordinated fragments. Moreover, substructure-matching tools are inherently designed to locate local motifs rather than to partition an entire molecular system into disjoint fragments, which was the objective of this analysis.

By constructing an explicit distance-based connectivity graph and identifying connected components, ESTRUCTURAL decomposed the system into desired fragments, including the heme group, coordinated and uncoordinated histidine residues, lysine, small ligands, and solvent molecules. This result highlights that ESTRUCTURAL does not rely rigidly on predefined tools, but can instead employ alternative computational strategies such as direct code-based reasoning, when these are better suited to the task at hand.

A similar pattern was observed in geometric operation tasks. While ESTRUCTURAL routinely employs geometric operation tools for single-step modifications of distances or angles, the agent adopted a custom Python-based approach when queried about a task requiring systematic batch generation of multiple structures. In the ferrocene distance and angle scan case study, the user requested a series of incremental geometric modifications, which generated multiple `xyz` files. Performing this workflow exclusively with single-operation geometry tools would have required numerous sequential tool invocations, introducing unnecessary overhead. Instead, the agent implemented vector-based geometric transformations within a Python execution environment, enabling efficient generation of the entire structure series in a single action. Notably, for isolated geometric modifications on ferrocene, the agent consistently employed the dedicated geometry operation tools, reflecting context-sensitive selection between specialized tools and direct code-based execution.

Taken together with the fragment analysis example, these examples illustrate that ESTRUCTURAL is not restricted to rigid tool usage, but dynamically evaluates task complexity, efficiency, and robustness when selecting an appropriate strategy. This flexibility represents a key strength of the agentic design.

### 3.2.6 Case study 6: Multimodal reaction mechanism-guided structure generation

Unlike organic-molecule specifications, reaction mechanisms involving intermediates and TSs are more commonly communicated through schematic images than through narrative text. This is because key geometric features of intermediates and TSs, such as distorted bond lengths, angles, and partially formed or broken bonds, are difficult to accurately describe using textual representations or string-based formats such as SMILES. In contrast, reaction mechanism diagrams can conveniently and intuitively convey these geometric and connectivity changes.

Motivated by this common practice, this case study evaluates the ability of ESTRUCTURAL to perform multimodal reasoning by generating three-dimensional molecular structures directly guided by a reaction mechanism schematic image (Figure 12). The target example is a migratory insertion reaction of ethylene into a metal–carbon bond, a key elementary step in ethylene polymerization (62, 63). The authors drew a schematic reaction mechanism to illustrate representative migratory insertion pathways involving transition-metal complexes.

To minimize explicit textual cues, annotations commonly included, such as Int1 (first intermediate) and TS1 (first transition state) labels, are intentionally omitted from the mechanism diagram. As a result, the image encodes the reaction pathway primarily through changes in coordination environment, metal–ligand connectivity, and the relative spatial arrangement of molecular fragments. This setup tests whether ESTRUCTURAL

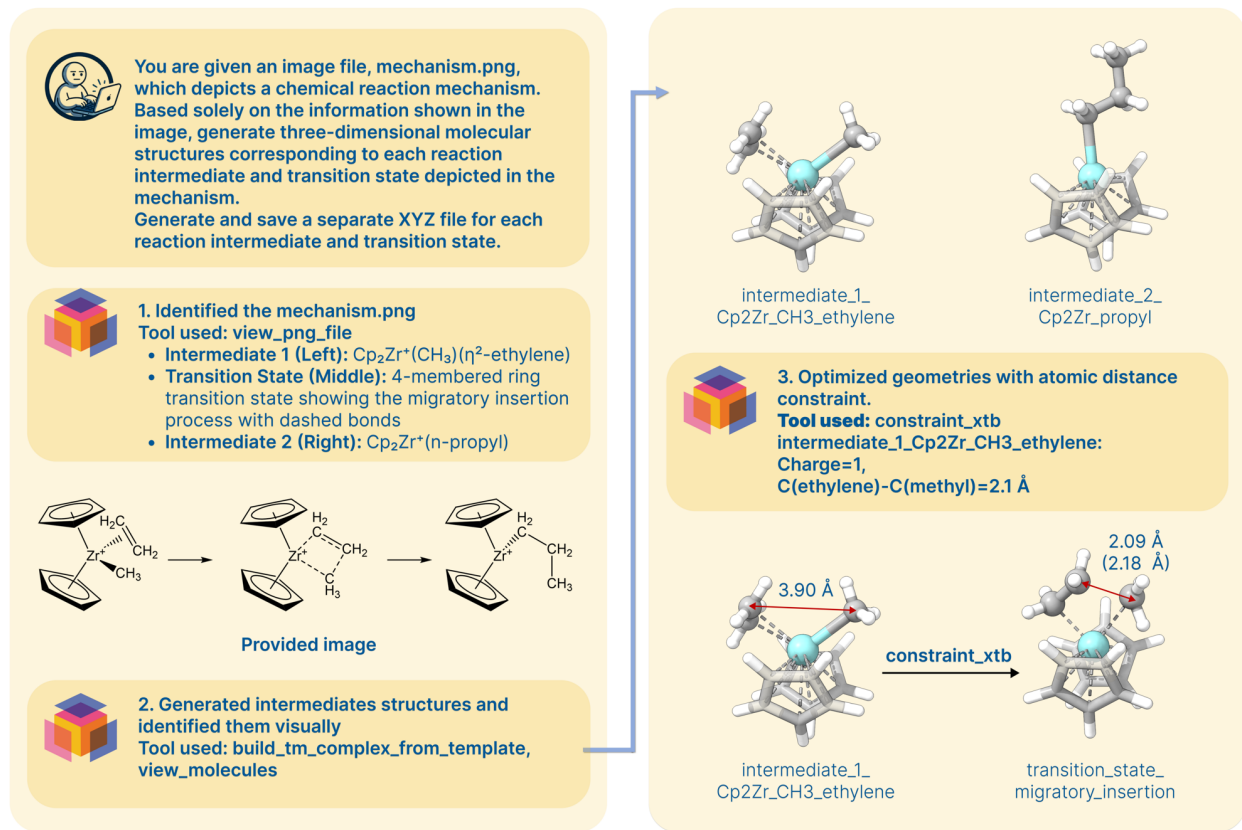


**Figure 12** Multimodal reaction mechanism-guided generation of intermediates and TS-like structures. Starting from a user prompt and a provided reaction mechanism image, ESTRUCTURAL identifies the reaction intermediates and TS motif, generates three-dimensional structures for each intermediate, and constructs TS-like geometry using the `constraint_xtb` tool. The highlighted interatomic C(ethylene)–C(methyl) distance is explicitly constrained during geometry optimization. The corresponding distances before and after constrained optimization are annotated for the generated intermediates and TS-like structure. For the optimized TS-like geometry, the value shown in parentheses denotes the reference distance obtained from an independent DFT transition-state optimization. Atom color codes: sky blue, Zr; gray, C; white, H.

can extract mechanistic and structural information directly from schematic visual input and translate it into chemically meaningful three-dimensional intermediates and transition-state geometries.

ESTRUCTURAL first analyzes the schematic reaction mechanism image and correctly identifies the catalytic system: a zirconocene complex coordinated to methyl and ethylene ligands. Based on the visual information, the agent labels the structure containing methyl and ethylene as intermediate 1, the propyl-bound structure as intermediate 2, and the ethylene migratory insertion configuration as the transition state. The generated geometries reproduce the coordination environments depicted in the schematic, yielding a tetrahedral zirconocene complex. The resulting two intermediate structures are consistent with the input image, in which the catalytic centers are coordinated by a methyl ligand and an ethylene ligand, respectively, and by a propyl ligand.

To construct TS geometries, ESTRUCTURAL employs the `constraint_xtb` tool to impose chemically reasonable interatomic distance constraints corresponding to the migratory insertion step. To evaluate the reasonableness of the generated TS-like structure, the constrained interatomic distance was compared against a reference value obtained from an independent DFT transition-state optimization at B3LYP-D4/def2-SVP level (64, 65, 66, 67, 68, 69) implemented in ORCA 6.0 (60). As shown in Figure 12, the constrained interatomic distance for the reacting atom pair is in close agreement with both optimized and reference TS geometry. ESTRUCTURAL imposes a distance constraint between the carbon atom of the methyl group and the reacting

carbon atom of ethylene of 2.10 Å. After constrained optimization, the corresponding C–C distances converge to 2.09 Å, which closely match the reference TS distances of 2.18 Å. Furthermore, full TS optimizations initiated from geometries generated by ESTRUCTURAL converged successfully, yielding transition states with a single imaginary frequency of  $-296\text{ cm}^{-1}$ . Throughout this process, ESTRUCTURAL dynamically combines visual inspection with explicit structural analysis tools to identify relevant atomic indices and guide geometry construction.

To evaluate the robustness of the workflow, we repeated the full procedure five times with the same prompt. The generation of the intermediates succeeded in all trials. In contrast, initial TS generation occasionally failed due to the ambiguous selection of the reacting carbon atom in ethylene. The agent sometimes selected either ethylene carbon at random, rather than the one closest to the metal-bound methyl group. Importantly, this failure mode was readily corrected through a brief interactive refinement. When provided with a follow-up prompt specifying that the reacting ethylene carbon should be the one closest to the methyl group, ESTRUCTURAL consistently recovered and generated the correct TS structure in all subsequent attempts (Figure S11).

This case study demonstrates that ESTRUCTURAL can integrate visual interpretation of reaction mechanisms with structure generation, editing, and geometric operations to produce chemically reasonable initial geometries for reaction intermediates and transition-state calculations. Beyond one-shot automation, the system also supports interactive, human-in-the-loop refinement, allowing errors arising from ambiguous geometric choices to be efficiently corrected. Such multimodal, image-guided, and interactive structure generation represents a significant step beyond text-only molecular specification and highlights the potential of ESTRUCTURAL to translate conceptual reaction mechanisms into explicit three-dimensional molecular models in a robust and user-aligned manner.

### 3.2.7 Case study 7: Mechanism reasoning driven geometry construction

A common challenge in reaction discovery campaigns in organic and organometallic chemistry is rationalizing reaction mechanisms to build an in-depth understanding and facilitate knowledge-driven experimental design, where computations can play a pivotal role.

Nevertheless, computing a chemical reaction diagram usually involves postulating the geometries of all ground and transition states involved in the chemical reactions. This can be laborious when handling multiple reaction sites and/or substituent patterns and is highly dependent on the operator’s thorough understanding of organic reaction mechanisms and computational chemistry skills. Taking the cutting-edge single atom skeletal editing reaction as an example (70), we illustrate the potential of ESTRUCTURAL for (1) following structures and substituent patterns in a reaction pathway, which is provided via text description or as an image using ball-and-stick model, (2) proposing transition-state formation mechanisms that are chemically sound and reconstructing the corresponding three-dimensional molecular structures as .xyz files, and (3) generating series of alternate reaction pathways with systematic structural modifications.

Specifically, we provided ESTRUCTURAL with an image of the reaction diagram in which the transition-state structure (path A) was masked, as shown in Figure 13a, and prompted it to generate a TS geometry. This challenged ESTRUCTURAL to infer a plausible TS formation mechanism and, following that hypothesis, construct a corresponding geometry. ESTRUCTURAL inferred an “SO extrusion + ring contraction” mechanism (Figure 13a) and translated this hypothesis into geometric constraints (S–C = 2.3 Å, S–N = 2.2 Å, and C–N = 1.9 Å), which are reasonable initial guesses close to the reference structure. ESTRUCTURAL further applied the same procedure to two alternative reaction pathways asked by the user to probe the preferred mechanism (Figure 13b,c,d).

Notably, while ESTRUCTURAL could recognize conservation of the substituent pattern on the ring before and after reaction, explicit instructions were necessary (e.g., specifying the R group on the carbon  $\alpha$  to S) to ensure consistent substitution across substrate and product structures. We also observed in previous trials that VLMs often fail to recognize even simple motifs (e.g., a six-membered ring) when the underlying mechanism is unclear, indicating perception failures on 2D reaction diagrams.

The structures generated by ESTRUCTURAL showcased C–N, S–N, and S–C distances of 1.88 Å, 2.09 Å, and 2.19 Å for path A, and 1.88 Å, 2.12 Å, and 2.18 Å for path B, respectively. We further validated the proposed

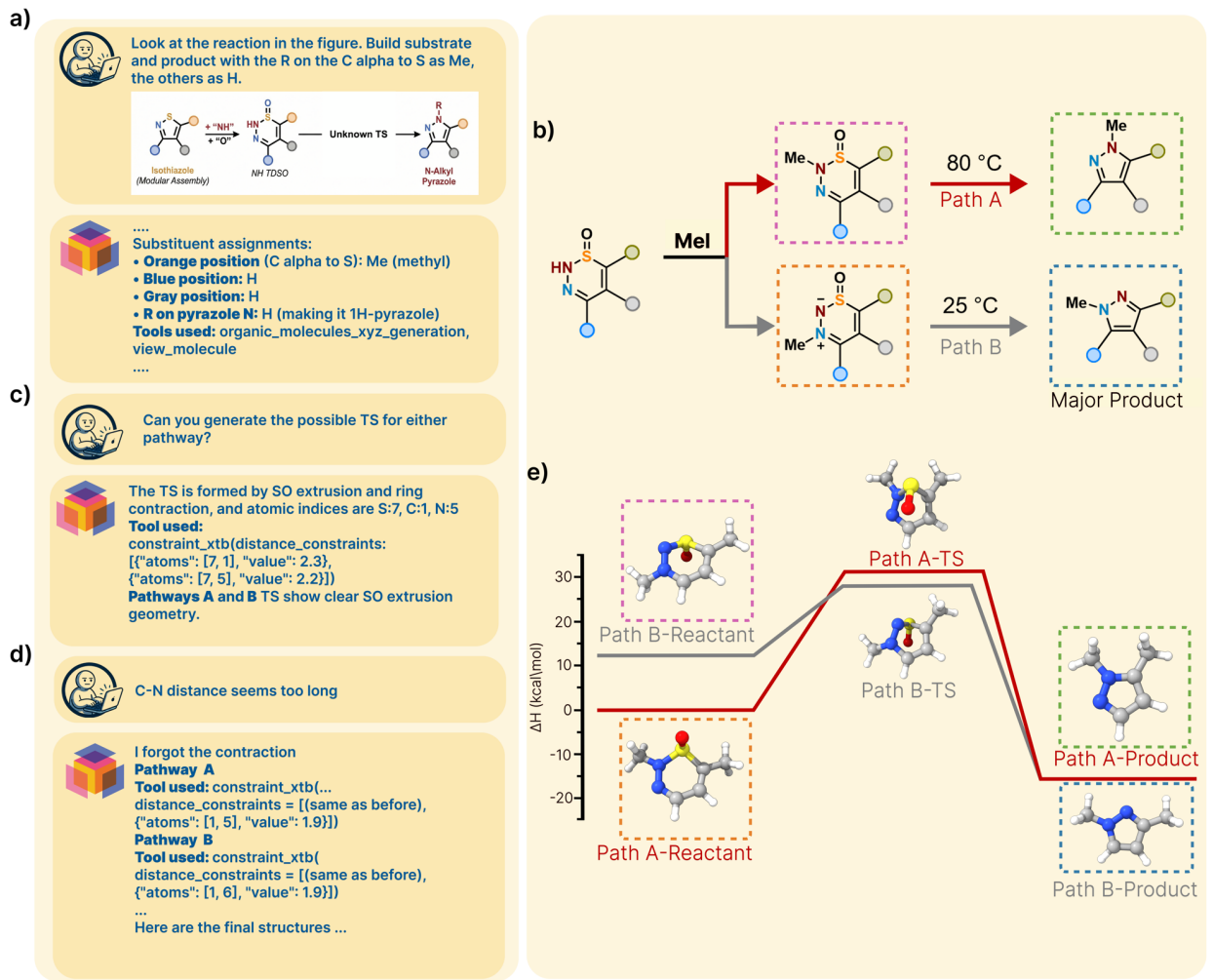


**Figure 13** Mechanism reasoning driven geometry construction. Starting from a provided reaction mechanism image with a masked transition state, ESTRUCTURAL generates three-dimensional structures for reactants, products, and transition states using the `constraint_xtb` tool. Moreover, it performs geometry construction of the reaction but with modified substituents, following user request. (a) User request for reactants and products geometries. (b) User request for TS structures. (c) Error recovery upon human feedback. (d) Chemical reaction pathways studied with ESTRUCTURAL. (e) Reaction energy profile at B3LYP-D4/def2-SVP level of theory calculated by the human expert using the geometries generated by ESTRUCTURAL. Atom color codes: yellow, S; red, O; blue, N; gray, C; white, H.

geometries by performing DFT calculations for the reactants, products, intermediates, and transition states, as shown in Figure 13e. The resulting trend is comparable to the energy profile reported in the literature (70). The full reaction energy diagram can be computed fully autonomously within EL AGENTE architecture (11), where EL AGENTE ESTRUCTURAL is connected to EL AGENTE QUINTUR (15), which allows autonomous end-to-end reaction pathway discovery and characterization.

Overall, this case study demonstrates how ESTRUCTURAL can support mechanistic investigation of consecutive reaction pathways by translating chemical hypotheses into concrete structural manipulations. At present, however, this is best viewed as a demonstration of emergent capability rather than evidence of robust performance across arbitrary reaction systems: current models often require substantial contextual prompting to reliably generate correct intermediates and transition states. Both perception and chemical reasoning remain key bottlenecks and likely require substantial advances to become reliable for this task, though rapid model advances may mitigate these limitations in the near future (Figure 14).

## 4 Discussion

In this section, we discuss the key strengths, limitations, and future development directions of EL AGENTE ESTRUCTURAL, together with a roadmap for its further extension.

### 4.1 Key strengths

#### 4.1.1 Structure preservation

A central strength of ESTRUCTURAL is its ability to manipulate molecular structures while preserving their underlying three-dimensional geometry. Instead of rebuilding structures from abstract representations, ESTRUCTURAL operates directly on existing geometries, enabling targeted modifications that reflect how chemists edit molecules in practice. This geometry-preserving approach is particularly important for systems that are sensitive to small structural changes, such as stereochemically complex molecules and coordination compounds, where unintended conformational or isomeric changes can arise from *de novo* generation.

By working directly with Cartesian coordinates, ESTRUCTURAL naturally supports a broad range of molecular systems, including organometallic complexes, weakly bound fragments, and other structures that are difficult to represent using string-based representation. This allows the agent to more reliably construct user-specified target structures while maintaining consistency of the molecular framework.

#### 4.1.2 Liquid workflows

Another distinguishing aspect of ESTRUCTURAL is its modular, tool-based architecture, which enables flexible composition of structure generation, editing, geometric operations, and structural analysis within a single workflow. Instead of relying on fixed, one-shot commands, our agent performs complex tasks through a sequence of connected steps that build on intermediate results, dynamically selecting analysis, generation, and geometric operations as required by the evolving task context. As demonstrated in the case studies, this design enables complex tasks such as site-selective functionalization, fragment-level replacement, and initial geometries for TS, requiring multiple tools to solve the query.

This flexibility also applies to the handling of molecular fragments. ESTRUCTURAL is not limited to a fixed library of predefined fragments. Although common functional groups and ligand templates are provided for convenience, the agent can generate and incorporate new molecular fragments on demand ([Figure 6](#) and [Figure 9](#)). This allows the system to adapt naturally to a wide range of chemical contexts and user requests that go beyond standard fragment libraries.

#### 4.1.3 Convert chemistry intent to 3D geometry

In addition, ESTRUCTURAL is able to translate high-level chemical intent into concrete geometric actions. Using structural analysis and chemical reasoning, the agent can automatically identify relevant atomic sites, symmetry-equivalent positions, and molecular fragments, enabling targeted modifications without requiring the user to manually specify atom indices. This capability is especially useful for organometallic systems and large molecular assemblies, where manual index selection and fragment identification are tedious and error-prone. By automating these low-level decisions, ESTRUCTURAL reduces the need for expert-driven manual intervention while still retaining precise control over structural changes.

#### 4.1.4 Multimodality

The multimodal vision capability demonstrated in Sections [3.2.6](#) and [3.2.7](#) highlights the extensibility of the framework beyond text-based inputs. By interpreting reaction mechanism schematics and translating visual information into explicit three-dimensional structures of reaction intermediates and transition states, ESTRUCTURAL demonstrates a capacity for multimodal reasoning that closely aligns with how chemists communicate mechanistic knowledge in practice. Taken together, these strengths position ESTRUCTURAL as a practical agent for interactive molecular modelling and structure preparation tasks in computational chemistry workflows.

#### 4.1.5 Interpretability

As ESTRUCTURAL proceeds with its agentic workflow, it plans and reasons about every move, providing the rationale and justification for every action and parameter setting. For example, as discussed in Section 3.2.7, ESTRUCTURAL proposes the TS formation rationale and translates it into a concrete setting of a distance constraint, with a clear explanation of the constraint selection: 2.2 Å for extrusion and 1.9 Å for contraction. Such explainability allows for a careful explanation of the geometry-formation logic and is highly deterministic, unlike in black-box systems.

## 4.2 Limitations and future directions

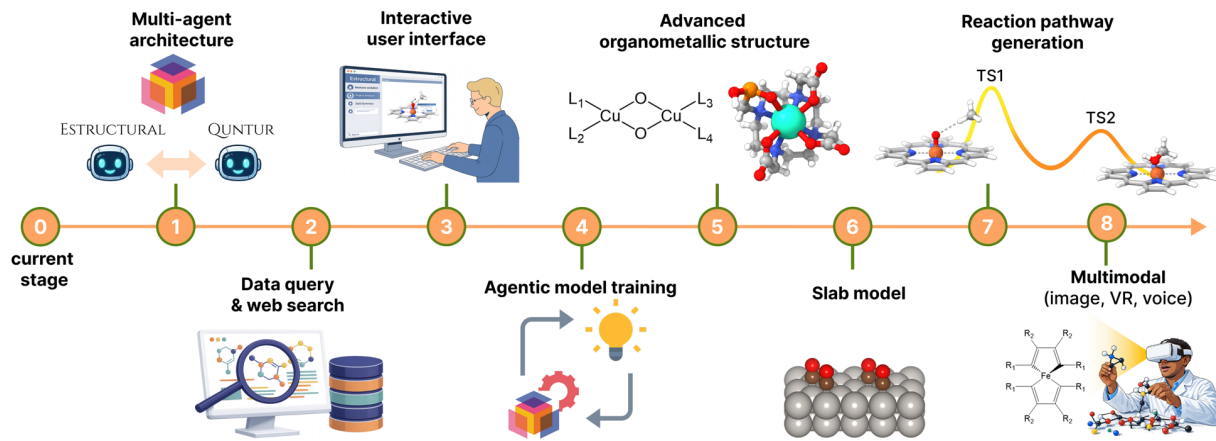


**Figure 14** Conceptual roadmap for future development of ESTRUCTURAL.

Despite its flexibility and broad applicability, ESTRUCTURAL exhibits several limitations that motivate future development efforts. Rather than viewing these limitations in isolation, we consider them as opportunities to further extend the scope, robustness, and practical impact of ESTRUCTURAL and its descendants. Building on the strengths and constraints identified in the preceding sections, we outline several future directions for ESTRUCTURAL (Figure 14). These directions are not intended to prescribe a strict development roadmap, but instead to highlight complementary and interrelated avenues through which the system can evolve, addressing current limitations while expanding its applicability to more complex and realistic computational chemistry workflows.

### 4.2.1 Integration with multi-agent quantum chemistry (Stage 1)

At present (Stage 0), ESTRUCTURAL is designed as a dedicated agent specialized in molecular structure generation, editing, and geometric manipulation, and does not perform electronic structure calculations itself. While this focused design enables robust, flexible control over molecular geometries, it also highlights a key limitation: structure preparation remains decoupled from downstream quantum-chemistry calculations. An important next step (Stage 1) is to integrate ESTRUCTURAL into our multi-agent quantum chemistry architecture, EL AGENTE QUNTRUR. Within this framework, ESTRUCTURAL can serve as a specialized geometry-manipulation agent that collaborates with other agents responsible for tasks such as a high-level planner, input-file generation, and DFT calculations. This integration enables EL AGENTE QUNTRUR to operate on user-demand structures across a substantially broader range of chemical systems, including stereochemically sensitive molecules, organometallic complexes, weakly bound intermediates, and catalytic reaction pathways involving intermediates and transition states.

### 4.2.2 Data-driven structure retrieval and editing (Stage 2)

Complementary to the construction of molecules from scratch, Stage 2 focuses on data-driven core-structure retrieval and editing. As illustrated in the case studies (Figure 10), editing an existing, chemically similar

structure is often more reliable than full *de novo* construction for large or highly coordinated organometallic systems. Future versions of ESTRUCTURAL will therefore incorporate data querying and web-search capabilities, enabling retrieval of relevant structures from the literature or curated databases—such as the Cambridge Structural Database (CSD) (71) and the Open Molecules 2025 (OMol25) dataset (72)—followed by targeted, geometry-preserving modifications. This hybrid strategy would further enhance the robustness and practicality of ESTRUCTURAL for real-world organometallic chemistry.

#### 4.2.3 Interactive user interfaces (Stage 3)

Although the current implementation of ESTRUCTURAL supports human-in-the-loop interaction through iterative natural language dialogue—allowing users to guide, correct, or refine the agent’s decisions—structural editing is currently mediated exclusively through language-based instructions and agent-executed operations. In practice, however, certain geometry-editing tasks can be more efficiently performed through direct user manipulation than through detailed natural language descriptions. For example, when a user intends to adjust the distance or angle between a specific pair of atoms within a large or complex molecule, directly selecting those atoms and applying the modification can be more intuitive and efficient than specifying the operation textually. Accordingly, an interactive user interface (UI) represents an important future direction for ESTRUCTURAL. Providing a visual editing environment in which users can directly select atoms and invoke existing structure-editing operations—such as substitution, distance tuning, or angle control—the system could seamlessly combine LLM-driven automation with familiar direct-manipulation workflows found in conventional molecular viewers. Such a hybrid interface would enhance usability and flexibility, enabling users to choose the most efficient interaction mode depending on the task, while complementing the agent’s autonomous capabilities in complex modeling workflows.

#### 4.2.4 Agentic model training on molecular manipulation (Stage 4)

Geometry manipulation tasks are clearly out of distribution for current vision–language models (VLMs). Two fundamental challenges remain. From a perception standpoint, VLMs lack the ability to reliably observe and analyze molecular systems, as discussed in 3.1. From a reasoning standpoint, existing systems have limited capacity to integrate chemical reasoning with spatial reasoning. Targeted agentic training will therefore be necessary to advance ESTRUCTURAL to the next level. Promising directions include synthetic data and task generation, as well as targeted post-training approaches such as reinforcement learning with verifiable rewards (RLVR)(73) and supervised fine-tuning (SFT)(74).

#### 4.2.5 Advanced organometallic structure construction (Stage 5)

While ESTRUCTURAL currently supports commonly used coordination geometries and ligand types, systems with very high coordination numbers (e.g., greater than six, as commonly encountered in lanthanide and actinide chemistry), multinuclear metal centers, or multiple polydentate ligands remain difficult to construct reliably using predefined templates alone. Promising directions include expanding the coordination-template library, developing more flexible rule-based construction strategies, and integrating external frameworks such as Architector (75) and molSimplify (76) as complementary tools to support the construction of more complex organometallic structures.

#### 4.2.6 Extension to slab models and solid-state systems (Stage 6)

The current implementation of ESTRUCTURAL is limited to molecular and coordination chemistry and does not yet support slab models or extended solid-state systems. Extending the framework to solids and surfaces represents Stage 6 of the roadmap. Supporting slab models, surface adsorption, and heterogeneous catalytic reactions will require explicit treatment of periodic boundary conditions, identification of adsorption sites (e.g., atop, bridge, and hollow), and extended coordination environments.

#### 4.2.7 Reaction pathway generation (Stage 7)

Extending ESTRUCTURAL toward systematic reaction pathway generation represents Stage 7 of the roadmap, building on the mechanism-guided case studies presented in this work. By generalizing image- and instruction-

guided structure construction to more complex reaction networks, ESTRUCTURAL could support the generation of consistent sets of reaction intermediates and TS-like structures, thereby providing structured initial geometries for downstream optimization, transition-state searches, and energy profiling. Furthermore, a future closed-loop workflow could couple agent-proposed mechanistic hypotheses, geometry construction for each hypothesis, and computational validation through quantum chemistry. Such a mechanism–geometry–validation loop could enable scalable, hypothesis-driven exploration of reaction space, allowing chemistry agents to tackle broader domains.

#### 4.2.8 Enhanced multimodal understanding and model improvement (Stage 8)

Many types of chemically relevant information are commonly communicated through schematic images rather than textual descriptions. In addition to reaction mechanisms, a series of functionalized derivatives derived from a common core structure is often presented visually. Such depictions can involve complex abstraction, including Markush structures or substitution patterns, which are difficult to encode solely with textual representations. Although ESTRUCTURAL already supports image-guided interpretation of reaction mechanisms, its ability to parse and reason over more abstract chemical diagrams remains limited. Enhancing multimodal understanding of these visual representations, therefore, represents an important direction for future development.

Beyond visual input, Stage 8 also envisions richer multimodal interaction modalities, including voice-based instructions (77, 78) and immersive interfaces such as virtual or augmented reality (79, 80, 81, 82, 83). Supporting these interaction modes would enable more intuitive and user-friendly control over molecular structure generation and editing, particularly for exploratory tasks where precise textual descriptions are cumbersome. Such interfaces can support education and training (84, 85, 86, 87) by enabling users to interactively explore molecular structures, reaction pathways, and stereochemical relationships in a more natural and accessible manner.

## 5 Conclusion

In this work, we introduce EL AGENTE ESTRUCTURAL, an agentic AI system that provides a natural-language–driven interface for comprehensive molecular-structure operations, including structure generation, editing, geometric operations, and analysis. By operating directly on three-dimensional Cartesian coordinates, ESTRUCTURAL enables modification of molecular structures following chemical intent while preserving their core geometry, beyond *de novo* generation. This capability is essential for modelling a broader spectrum of chemically relevant structures, including reaction intermediates, transition-state-like geometries, and coordination complexes that are difficult to access using conventional string-based approaches.

Through a series of realistic case studies, we demonstrated that combining large language model reasoning with structure-manipulation tools, explicitly designed to mirror how computational chemists manipulate structures in practice, enables users to solve practically relevant structure-manipulation tasks in computational chemistry, such as site-selective functionalization, fragment binding, and stereochemically controlled editing. As a result, ESTRUCTURAL offers a practical and reliable pathway for preparing input geometries within automated and semi-autonomous computational chemistry workflows.

Continued development of ESTRUCTURAL, together with its integration into EL AGENTE QUNTUR, is expected to facilitate increasingly autonomous exploration of chemical space spanning molecular, organometallic, and catalysis. We anticipate that such agentic approaches will play an important role in facilitating more robust and reliable automated computational workflows, ultimately accelerating discovery and advancing our understanding across a wide range of chemical systems.

## Data Availability

All data for the case studies are published at <https://github.com/aspuru-guzik-group/ElAgenteEstructuralCaseStudies>.

## Acknowledgments

We gratefully acknowledge the longstanding contributions of the Matter Lab's current and past group members ([matter.toronto.edu](http://matter.toronto.edu)), and in particular from El Agente team ([elagente.ca](http://elagente.ca)). C.C. acknowledges support from the DOE grant with the University of Minnesota award #A006801504 and the Basic Science Research Program through the National Research Foundation of Korea (NRF) funded by the Ministry of Education (RS-2025-02634334). Y.K. was supported by the CIFAR AI Safety Catalyst Award (Catalyst Fund Project #CF26-AI-001). J.B.P.S. acknowledges funding of this project by the National Sciences and Engineering Research Council of Canada (NSERC) Alliance Grant #ALLRP587593-23 (Quantamole). This research is part of the University of Toronto's Acceleration Consortium, which receives funding from the CFREF-2022-00042 Canada First Research Excellence Fund. Computations were performed on the Niagara supercomputer at the SciNet HPC Consortium. SciNet is funded by: the Canada Foundation for Innovation; the Government of Ontario; Ontario Research Fund - Research Excellence; and the University of Toronto. A.A.-G. thanks Anders G. Frøseth, for his generous support. A.A.-G. and V.B. acknowledge the generous support of Natural Resources Canada and the Canada 150 Research Chairs program and the University of Toronto's Acceleration Consortium, which receives funding from the CFREF-2022-00042 Canada First Research Excellence Fund. This work was supported by the AI2050 program of Schmidt Sciences. Molecular graphics and analyses were performed with UCSF ChimeraX (45, 46), developed by the Resource for Biocomputing, Visualization, and Informatics at the University of California, San Francisco, with support from National Institutes of Health R01-GM129325 and the Office of Cyber Infrastructure and Computational Biology, National Institute of Allergy and Infectious Diseases.

## References

- [1] Houk, K. & Liu, F. Holy grails for computational organic chemistry and biochemistry. *Acc. Chem. Res.* **50**, 539–543 (2017).
- [2] Nørskov, J. K., Bligaard, T., Rossmeisl, J. & Christensen, C. H. Towards the computational design of solid catalysts. *Nat. Chem.* **1**, 37–46 (2009).
- [3] Huang, B., von Rudorff, G. F. & von Lilienfeld, O. A. The central role of density functional theory in the ai age. *Science* **381**, 170–175 (2023).
- [4] Gómez-Bombarelli, R. *et al.* Design of efficient molecular organic light-emitting diodes by a high-throughput virtual screening and experimental approach. *Nat. Mater.* **15**, 1120–1127 (2016).
- [5] Greeley, J., Jaramillo, T. F., Bonde, J., Chorkendorff, I. & Nørskov, J. K. Computational high-throughput screening of electrocatalytic materials for hydrogen evolution. *Nat. Mater.* **5**, 909–913 (2006).
- [6] Seh, Z. W. *et al.* Combining theory and experiment in electrocatalysis: Insights into materials design. *Science* **355**, eaad4998 (2017).
- [7] Gu, G. H. *et al.* Progress in computational and machine-learning methods for heterogeneous small-molecule activation. *Adv. Mater.* **32**, 1907865 (2020).
- [8] Greeley, J. *et al.* Alloys of platinum and early transition metals as oxygen reduction electrocatalysts. *Nat. Chem.* **1**, 552–556 (2009).
- [9] Garza, A. J., Bell, A. T. & Head-Gordon, M. Mechanism of CO<sub>2</sub> reduction at copper surfaces: pathways to C<sub>2</sub> products. *ACS. Catal.* **8**, 1490–1499 (2018).
- [10] Peterson, A. A., Abild-Pedersen, F., Studt, F., Rossmeisl, J. & Nørskov, J. K. How copper catalyzes the electroreduction of carbon dioxide into hydrocarbon fuels. *Energy Environ. Sci.* **3**, 1311–1315 (2010).
- [11] Zou, Y. *et al.* El agente: An autonomous agent for quantum chemistry. *Matter* **8**, 102263 (2025).
- [12] Pham, T. D., Tamikanti, A. & Keçeli, M. Chemgraph: An agentic framework for computational chemistry workflows. *arXiv* (2025). arXiv:2506.06363 [physics.chem-ph].
- [13] Hu, J. *et al.* Aitomia: Your intelligent assistant for ai-driven atomistic and quantum chemical simulations (2025). arXiv:2505.08195 [physics.comp-ph].
- [14] Wang, Z. *et al.* Dreams: Density functional theory based research engine for agentic materials simulation (2025). arXiv:2507.14267 [cs.AI].
- [15] Pérez-Sánchez, J. B. *et al.* El Agente Quntur: A research collaborator agent for quantum chemistry (2026). Manuscript in preparation.
- [16] Bento, A. P. *et al.* An open source chemical structure curation pipeline using rdkit. *J. Cheminform.* **12**, 51 (2020).
- [17] O’Boyle, N. M. *et al.* Open babel: An open chemical toolbox. *J. Cheminform.* **3**, 33 (2011).
- [18] Gómez-Bombarelli, R. *et al.* Automatic Chemical Design Using a Data-Driven Continuous Representation of Molecules. *ACS Cent. Sci.* **4**, 268–276 (2018).
- [19] Segler, M. H., Kogej, T., Tyrchan, C. & Waller, M. P. Generating focused molecule libraries for drug discovery with recurrent neural networks. *ACS Cent. Sci.* **4**, 120–131 (2018).
- [20] Gupta, A. *et al.* Generative recurrent networks for de novo drug design. *Mol. Inf.* **37**, 1700111 (2018).
- [21] Popova, M., Isayev, O. & Tropsha, A. Deep reinforcement learning for de novo drug design. *Sci. Adv.* **4**, eaap7885 (2018).
- [22] Sanchez-Lengeling, B. & Aspuru-Guzik, A. Inverse molecular design using machine learning: Generative models for matter engineering. *Science* **361**, 360–365 (2018).
- [23] Ramakrishnan, R., Dral, P. O., Rupp, M. & Von Lilienfeld, O. A. Quantum chemistry structures and properties of 134 kilo molecules. *Sci. data* **1**, 1–7 (2014).
- [24] Krenn, M. *et al.* Selfies and the future of molecular string representations. *Patterns* **3** (2022).

[25] Hanwell, M. D. *et al.* Avogadro: an advanced semantic chemical editor, visualization, and analysis platform. *J. Cheminform.* **4**, 17 (2012).

[26] Dennington, R., Keith, T. A. & Millam, J. M. Gaussview Version 6 (2019). Semichem Inc. Shawnee Mission KS.

[27] Gilbert, A. Iqmol: A molecular builder and visualization package.

[28] Schaftenaar, G. & Noordik, J. H. Molden: a pre-and post-processing program for molecular and electronic structures. *J. Comput. Aided Mol. Des.* **14**, 123–134 (2000).

[29] Chemcraft - graphical software for visualization of quantum chemistry computations. version 1.8, build 682.

[30] Li, J. & Lai, L. SynCraft: Guiding Large Language Models to Predict Edit Sequences for Molecular Synthesizability Optimization (2025). arXiv:2512.20333 [cs.AI].

[31] Lv, T. *et al.* AtomWorld: A Benchmark for Evaluating Spatial Reasoning in Large Language Models on Crystalline Materials (2025). arXiv:2510.04704 [cond-mat].

[32] Sumers, T., Yao, S., Narasimhan, K. & Griffiths, T. Cognitive architectures for language agents. *Transactions on Machine Learning Research* (2023).

[33] Larsen, A. H. *et al.* The atomic simulation environment—a Python library for working with atoms. *J. Phys. Condens. Matter* **29**, 273002 (2017).

[34] Togo, A., Shinohara, K. & Tanaka, I. Spglib: a software library for crystal symmetry search. *Sci. Technol. Adv. Mater.* **4**, 2384822 (2024).

[35] Ong, S. P. *et al.* Python materials genomics (pymatgen): A robust, open-source python library for materials analysis. *Comput. Mater. Sci.* **68**, 314–319 (2013).

[36] Bannwarth, C., Ehler, S. & Grimme, S. GFN2-xTB - An Accurate and Broadly Parametrized Self-Consistent Tight-Binding Quantum Chemical Method with Multipole Electrostatics and Density-Dependent Dispersion Contributions. *J. Chem. Theory Comput.* **15**, 1652–1671 (2019).

[37] Bannwarth, C. *et al.* Extended tight-binding quantum chemistry methods. *Wiley Interdiscip. Rev. Comput. Mol. Sci.* **11**, 1–49 (2021).

[38] Spicher, S. & Grimme, S. Robust Atomistic Modeling of Materials, Organometallic, and Biochemical Systems. *Angew. Chem. Int. Ed.* **132**, 15795–15803 (2020).

[39] Grimme, S., Bannwarth, C. & Shushkov, P. A Robust and Accurate Tight-Binding Quantum Chemical Method for Structures, Vibrational Frequencies, and Noncovalent Interactions of Large Molecular Systems Parametrized for All spd-Block Elements (Z = 1–86). *J. Chem. Theory Comput.* **13**, 1989–2009 (2017).

[40] Schrödinger, LLC. The PyMOL molecular graphics system, version 1.8 (2015).

[41] Kim, S. *et al.* Pubchem 2025 update. *Nucleic Acids Res.* **53**, D1516–D1525 (2025).

[42] Axelrod, S. & Gómez-Bombarelli, R. GEOM, energy-annotated molecular conformations for property prediction and molecular generation. *Sci. Data* **9** (2022).

[43] Narayanan, S. M. *et al.* Training a Scientific Reasoning Model for Chemistry (2025). arXiv:2506.17238 [cs].

[44] Li, J. *et al.* Chemvlm: Exploring the power of multimodal large language models in chemistry area. In *Proceedings of the AAAI Conference on Artificial Intelligence*, vol. 39, 415–423 (2025).

[45] Pettersen, E. F. *et al.* Ucsf chimeraX: Structure visualization for researchers, educators, and developers. *Protein Sci.* **30**, 70–82 (2021).

[46] Meng, E. C. *et al.* UCSF ChimeraX: Tools for structure building and analysis. *Protein Sci.* **32**, e4792 (2023).

[47] Imai, M., Masaoka, S. & Kondo, M. Function provision to fe–porphyrin complexes for CO<sub>2</sub> reduction. *JACS Au* **5**, 3716–3737 (2025).

[48] Yu, S. *et al.* CO<sub>2</sub>-to-methanol electroconversion on a molecular cobalt catalyst facilitated by acidic cations. *Nat. Catal.* **7**, 1000–1009 (2024).

[49] Han, N. *et al.* Supported cobalt polyphthalocyanine for high-performance electrocatalytic CO<sub>2</sub> reduction. *Chem* **3**, 652–664 (2017).

[50] Zhu, Q. *et al.* The solvation environment of molecularly dispersed cobalt phthalocyanine determines methanol selectivity during electrocatalytic CO<sub>2</sub> reduction. *Nat. Catal.* **7**, 987–999 (2024).

[51] Su, J. *et al.* Strain enhances the activity of molecular electrocatalysts via carbon nanotube supports. *Nat. Catal.* **6**, 818–828 (2023).

[52] Lee, B.-H. *et al.* Supramolecular tuning of supported metal phthalocyanine catalysts for hydrogen peroxide electrosynthesis. *Nat. Catal.* **6**, 234–243 (2023).

[53] Liu, Y. & McCrory, C. C. Modulating the mechanism of electrocatalytic CO<sub>2</sub> reduction by cobalt phthalocyanine through polymer coordination and encapsulation. *Nat. Commun.* **10**, 1683 (2019).

[54] Fan, W. *et al.* Rational design of heterogenized molecular phthalocyanine hybrid single-atom electrocatalyst towards two-electron oxygen reduction. *Nat. Commun.* **14**, 1426 (2023).

[55] Nandy, A., Duan, C., Goffinet, C. & Kulik, H. J. New strategies for direct methane-to-methanol conversion from active learning exploration of 16 million catalysts. *JACS Au* **2**, 1200–1213 (2022).

[56] Bursch, M. *et al.* Understanding and quantifying london dispersion effects in organometallic complexes. *Acc. Chem. Res.* **52**, 258–266 (2018).

[57] Arashiba, K., Miyake, Y. & Nishibayashi, Y. A molybdenum complex bearing PNP-type pincer ligands leads to the catalytic reduction of dinitrogen into ammonia. *Nat. Chem.* **3**, 120–125 (2011).

[58] Kuramochi, H. *et al.* Ultrafast Raman observation of the perpendicular intermediate phantom state of stilbene photoisomerization. *Nat. Chem.* **16**, 22–27 (2024).

[59] Villarón, D. & Wezenberg, S. J. Stiff-stilbene photoswitches: from fundamental studies to emergent applications. *Angew. Chem. Int. Ed.* **132**, 13292–13302 (2020).

[60] Neese, F. Software update: The ORCA program system—version 6.0. *Wiley Interdiscip. Rev. Comput. Mol. Sci.* **15**, e70019 (2025).

[61] Neese, F. *ORCA 6.0 Manual*. Max-Planck-Institut für Kohlenforschung (2025). Version 6.0.

[62] Alt, H. G. & Köppl, A. Effect of the nature of metallocene complexes of group iv metals on their performance in catalytic ethylene and propylene polymerization. *Chem. Rev.* **100**, 1205–1222 (2000).

[63] Musaev, D. G., Froese, R. D., Svensson, M. & Morokuma, K. A density functional study of the mechanism of the diimine- nickel-catalyzed ethylene polymerization reaction. *J. Am. Chem. Soc.* **119**, 367–374 (1997).

[64] Becke, A. D. Density-functional thermochemistry. III. The role of exact exchange. *J. Chem. Phys.* **98**, 5648–5652 (1993).

[65] Lee, C., Yang, W. & Parr, R. G. Development of the Colle-Salvetti correlation-energy formula into a functional of the electron density. *Physical Review B* **37**, 785–789 (1988).

[66] Stephens, P. J., Devlin, F. J., Chabalowski, C. F. & Frisch, M. J. Ab Initio Calculation of Vibrational Absorption and Circular Dichroism Spectra Using Density Functional Force Fields. *J. Phys. Chem.* **98**, 11623–11627 (1994).

[67] Caldeweyher, E., Bannwarth, C. & Grimme, S. Extension of the d3 dispersion coefficient model. *J. Chem. Phys.* **147** (2017).

[68] Caldeweyher, E. *et al.* A generally applicable atomic-charge dependent London dispersion correction. *J. Chem. Phys.* **150**, 154122 (2019).

[69] Weigend, F. & Ahlrichs, R. Balanced basis sets of split valence, triple zeta valence and quadruple zeta valence quality for H to Rn: Design and assessment of accuracy. *Phys. Chem. Chem. Phys.* **7**, 3297–3305 (2005).

[70] Fanourakis, A. *et al.* Strategic atom replacement enables regiocontrol in pyrazole alkylation. *Nature* **641**, 646–652 (2025).

[71] Groom, C. R., Bruno, I. J., Lightfoot, M. P. & Ward, S. C. The cambridge structural database. *Acta Crystallogr. Sect. B Struct. Sci. Cryst. Eng. Mater.* **72**, 171–179 (2016).

[72] Levine, D. S. *et al.* The open molecules 2025 (omol25) dataset, evaluations, and models (2025). arXiv:2505.08762 [physics.chem-ph].

[73] Guo, D. *et al.* DeepSeek-R1 incentivizes reasoning in LLMs through reinforcement learning. *Nature* **645**, 633–638 (2025).

[74] Ouyang, L. *et al.* Training language models to follow instructions with human feedback. *Advances in neural information processing systems* **35**, 27730–27744 (2022).

[75] Taylor, M. G. *et al.* Architector for high-throughput cross-periodic table 3D complex building. *Nat. Commun.* **14**, 2786 (2023).

[76] Terrones, G. *et al.* molSimplify 2.0: Improved structure generation for automating discovery in inorganic molecular and reticular chemistry (2025). chemrxiv-2025-h8gff-v2.

[77] Darvish, K. *et al.* Organa: A robotic assistant for automated chemistry experimentation and characterization. *Matter* **8** (2025).

[78] Raucci, U. *et al.* Voice-controlled quantum chemistry. *Nat. Comput. Sci.* **1**, 42–45 (2021).

[79] Aspuru-Guzik, A., Lindh, R. & Reiher, M. The matter simulation (R)evolution. *ACS Cent. Sci.* **4**, 144–152 (2018).

[80] Taylor, M. V. *et al.* Optimising digital twin laboratories with conversational ais: enhancing immersive training and simulation through virtual reality. *Digital Discovery* **4**, 1134–1141 (2025).

[81] O'Connor, M. *et al.* Sampling molecular conformations and dynamics in a multiuser virtual reality framework. *Sci. Adv.* **4**, eaat2731 (2018).

[82] Baaden, M. & Glowacki, D. R. Virtual reality in drug design: Benefits, applications and industrial perspectives. *Curr. Opin. Struct. Biol.* **92**, 103044 (2025).

[83] Marti, K. H. & Reiher, M. Haptic quantum chemistry. *J. Comput. Chem.* **30**, 2010–2020 (2009).

[84] Fombona-Pascual, A., Fombona, J. & Vázquez-Cano, E. VR in chemistry, a review of scientific research on advanced atomic/molecular visualization. *Chem. Educ. Res. Pract.* **23**, 300–312 (2022).

[85] Bennie, S. J. *et al.* Teaching enzyme catalysis using interactive molecular dynamics in virtual reality. *J. Chem. Educ.* **96**, 2488–2496 (2019).

[86] Taylor, M. *et al.* Breaking the access to education barrier: enhancing hplc learning with virtual reality. *J. Chem. Educ.* **101**, 4093–4101 (2024).

[87] Sohail, M., Habib, U. & Rasool, S. VR stereo thrills & spills: An immersive virtual reality game for enhancing student understanding of stereoisomerism. *J. Chem. Educ.* **102**, 2002–2012 (2025).

# Supporting Information

## A Agents and Tools

In this section, we summarize the agents and tools developed as part of ESTRUCTURAL.

**Table S1** Summary of agents and tools.

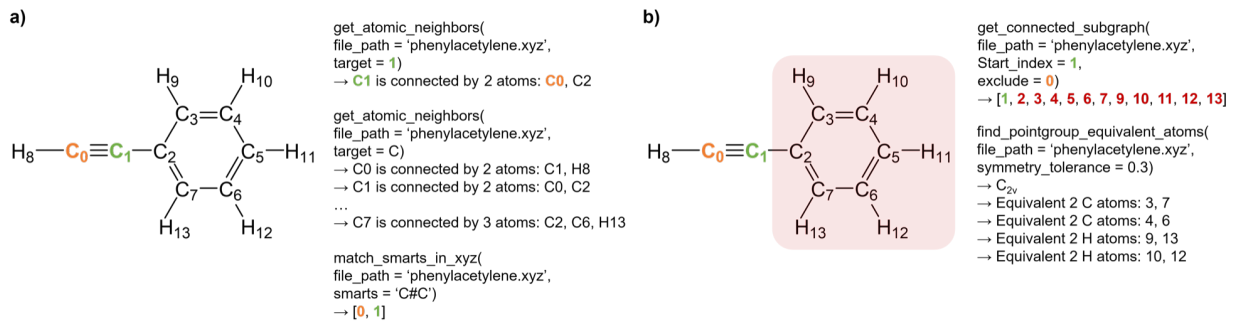
Label / LLM model	Description
geometry_operator	Responsible for high-level structure manipulation tasks, including planning and executing actions such as geometry generation, editing, analysis, and other operations.
python_repl	Accesses a Python terminal to run Python code and interacts with the local machine as needed.
png_viewer	View a PNG image file.
find_available_fragments	Search available predefined fragments.
replace_terminal_atoms_with_fragment	Connect two XYZ structures at specified atomic indices.
replace_terminal_atom_with_predefined_FG	Replace atomic indices in XYZ file with a certain predefined fragment.
bind_two_molecules	Attach a certain XYZ structure to specified atomic indices.
bind_predefined_fragment	Bind a predefined fragment to the provided atomic indices in the XYZ file.
bind_atom_ligands_library	Bind a predefined fragment to the provided element in the XYZ file.
replace_branch_with_predefined_FG	Replace molecular branches connected to a specified atomic index with another branch from predefined fragments.
replace_branch	Replace a molecular branch in one XYZ with another XYZ file.
build_tm_complex_from_template	Build transition metal complex from predefined templates.
build_predefined_organometallic	Build predefined organometallic complexes.
organic_molecules_xyz_generation	Generates XYZ files for organic molecules from a list of SMILES strings using RDKit for 3D structure generation.
move_atoms	Move selected atomic indices by a specified vector.
get_distance_angle_dihedral	Get distance, angle, and dihedral defined by selected atomic indices.
set_distance_between_fragments	Set distance between two selected atomic indices (or involved fragments).
set_angle_between_fragments	Set angle defined by three selected atomic indices (or involved fragments).
set_dihedral_between_fragments	Set dihedral angle defined by four selected atomic indices (or involved fragments).
remove_atoms	Remove selected atomic indices from the XYZ file.

Table S1 – continued from previous page

Label	Description
rotate_substituents_around_bisector	Rotate a group of atoms around the connected atom bisector.
insert_atom_at_centroid	Insert an atom at the centroid of selected atomic indices.
get_atomic_neighbors	Find neighboring atoms for a given element symbol or atomic index.
match_smarts_in_xyz	Match SMARTS patterns in the XYZ file and return the corresponding atomic indices (without H atoms).
get_connected_subgraph_indices	Get all atomic indices connected to a specified atomic index.
find_pointgroup_equivalent_atoms	Find equivalent atoms in the molecule based on point group symmetry.
constraint_xtb	Conducts a geometry optimization using GFN $n$ -xTB or GFN-FF. Optionally, force constants on specific angles, torsions, and distances can be set.
lookup_smiles_from_name	Lookup SMILES string from common chemical name using PubChem database.

## B Supplementary Notes on Tool Implementation

### B.1 Structural Analysis Tools



**Figure S1** Overview of the analysis tools, their input arguments, and the returned results. For each example, the input molecular structure and specified arguments are shown together with the corresponding outputs produced by the analysis tools. The illustrated cases include (a) `get_atomic_neighbors`, `match_smarts_in_xyz`, (b) `get_connected_subgraph` and `find_pointgroup_equivalent_atoms`.

`get_atomic_neighbors` tool takes an XYZ file and a `target` argument, which can be specified either as an atomic index (integer) or as an element symbol. If the target is provided as an atomic index, the tool returns a list of atoms directly bonded to the target atom, together with their element types and atomic indices. If the target is specified as an element symbol, the tool identifies all atoms of the given element in the structure and returns, for each such atom, its neighboring atoms along with their element types and indices.

`match_smarts_in_xyz` tool first converts the input XYZ file into a MOL object, from which molecular connectivity is inferred. Based on this connectivity, the tool identifies atomic indices that match the input SMILES or SMARTS pattern. Hydrogen atoms are excluded from the matching results.

`get_connected_subgraph` tool requires two arguments: `start_index` and `exclude`. Starting from the atom specified by `start_index`, the tool identifies all atoms in the connected subgraph while traversing the molecular graph in the direction opposite to the excluded atom. Therefore, the `start_index` and the `exclude` atom must be directly bonded to each other. The output is a list of atomic indices belonging to the identified subgraph.

`find_pointgroup_equivalent_atoms` tool takes an XYZ file and a symmetry tolerance as input. In this work, the symmetry tolerance is set to 0.3 Å, which corresponds to the default value used in `pymatgen`. Using this tolerance, the tool determines the molecular point group and returns lists of symmetrically equivalent atoms with their corresponding atomic indices.

Point-group detection is sensitive to both the numerical tolerance and the spatial orientation of atoms in the molecular geometry. To improve robustness, the tool internally performs additional point-group analyses using a looser tolerance (0.5 Å, increased by 0.2 Å from the default) and by repeating the analysis after removing hydrogen atoms. If the point group detected using the default tolerance differs from that obtained using the looser tolerance or from the hydrogen-removed structure, the tool reports the discrepancy and recommends using a looser symmetry tolerance.

## B.2 Geometric Operation Tools

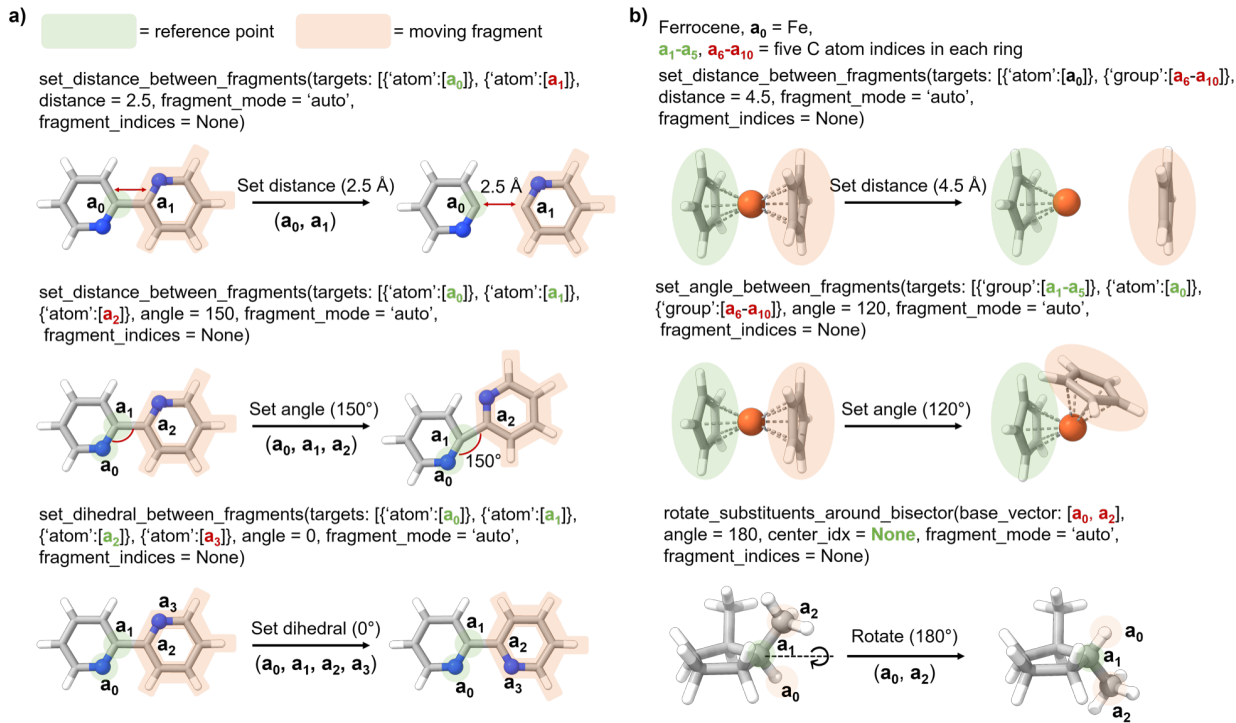


**Figure S2** Overview of geometric operation tools in ESTRUCTURAL. (a) Atom-based operations, (b) group-based operations and rotation. Each example shows the initial molecular structure, the applied geometric operation with its input parameters, and the resulting structure after the operation. The operations include distance, angle, dihedral control, and fragment rotation.

### Operation tools: distance, angle, dihedral, and rotation

The geometric operation tools in ESTRUCTURAL enable direct control of interatomic distances, angles, dihedral angles, and fragment rotations while preserving the internal geometry of unaffected regions. These operations are defined through a flexible target specification and fragment-handling scheme, allowing both atom-level and fragment-level manipulation.

### Target specification and dummy atom construction

Geometric operations are specified using a `targets` dictionary. For atom-level operations, a target is defined by a single atomic index. For group-level operations, the target is defined as a list of atomic indices corresponding to a molecular fragment or functional group. In this case, a dummy atom is introduced at the centroid of the specified indices, and this centroid is used as the effective reference point for geometric control.

Distances, angles, and dihedral angles are then evaluated and manipulated using these atomic or centroid-based reference points, allowing consistent treatment of both individual atoms and extended groups within a unified framework.

### Fragment selection modes

To determine which atoms are displaced during a geometric operation, geometric operation tools support three fragment selection modes via the `fragment_mode` parameter:

`fragment_mode = 'auto'` The moving fragment is automatically identified based on molecular connectivity. For example, when modifying the distance between atoms a<sub>0</sub> and a<sub>1</sub>, the algorithm identifies all atoms belonging to the branch extending from a<sub>1</sub> in the direction opposite to a<sub>0</sub>. This is achieved using a connectivity-based

subgroup detection procedure (via `get_subgroup_indices`). The entire detected fragment is then displaced collectively.

`fragment_mode = 'manual'` The user explicitly specifies the indices of atoms to be moved via `fragment_indices`. This mode provides full control when automatic fragment detection is ambiguous or when custom selections are required.

`fragment_mode = 'none'` Only the explicitly specified atom or group indices are displaced, without any automatic expansion to connected atoms.

### **Rotation operations**

Rotation operations are defined by specifying a set of `base_vector_indices`, which determine the rotation axis and reference direction. Let these indices correspond to atoms  $a_1, a_2, \dots, a_n$ . The rotation center, denoted as  $a_0$ , is identified as the atom that is commonly bonded to all atoms in `base_vector_indices`. If not explicitly provided via `center_idx`, this atom is automatically inferred from molecular connectivity.

For each base atom  $a_i$ , a unit vector  $\hat{v}_i = (a_i - a_0)/|a_i - a_0|$  is constructed. These unit vectors are summed and normalized to define the effective rotation axis. Atoms in the selected fragment are then rotated by the target angle around this axis, with the same `fragment_mode` and `fragment_indices` logic applied as in distance and angle operations. These operation tools generalize common manual manipulations performed in molecular viewers into programmatic actions that can be invoked by the agent.

### B.3 Structural Editing Tools

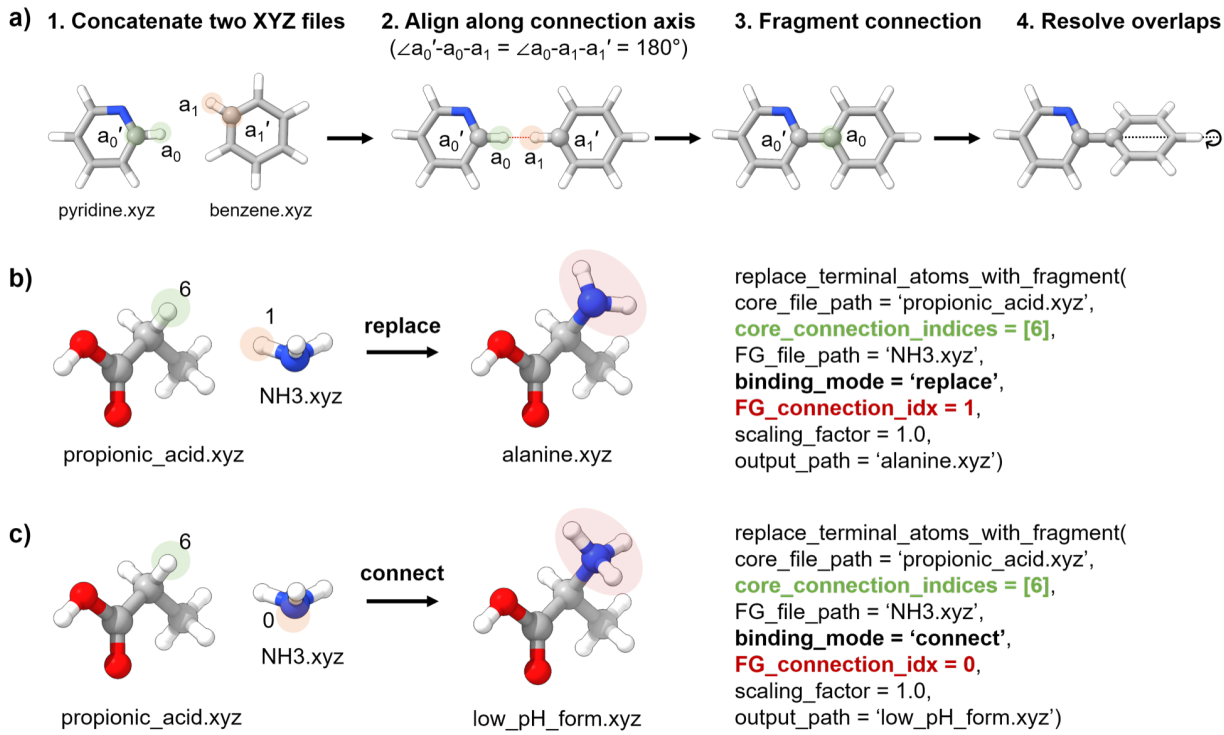


**Figure S3** Detailed mechanism and arguments of `replace_terminal_atoms_with_fragment` tool. (a) Schematic workflow for the replacement tool. The initial molecular structure, the applied replacement with its input parameters, and the resulting structure after the operation for (b) `binding_mode` = ‘replace’, and (c) `binding_mode` = ‘connect’. Here,  $a_0$  and  $a_1$  denote the terminal atoms selected as substitution sites in the two structures. Since both are terminal, each is bonded to a single neighboring atom, denoted as  $a_0'$  and  $a_1'$ , respectively. Atom color codes: red, O; blue, N; gray, C; white, H.

#### Core-substituent attachment using terminal connection indices

The input arguments include a core structure file (`core_file_path`) and a list of terminal connection indices, `core_connection_indices` =  $\{a_0\}$ , which specifies the terminal atoms in the core to be replaced (typically H atoms). For each specified terminal atom  $a_0$ , its directly bonded neighbor in the core is determined internally and denoted as  $a_0'$ .

A substituent fragment is provided separately. Based on the user prompt, the agent identifies the terminal attachment atom in the substituent, which is denoted as  $a_1$ . The unique bonded neighbor of  $a_1$  within the substituent is then determined internally by the tool and denoted as  $a_1'$ .

In the case of `binding_mode` = ‘connect’, the substituent fragment is attached without removing the fragment-side connection atom. Instead, a dummy atom is introduced at the fragment connection site according to the local VSEPR geometry (Figure S4), as discussed in detail in the following section. The newly introduced dummy atom is treated as the terminal attachment atom  $a_1$ , while the originally specified fragment connection index (`FG_connection_idx`) is treated as its bonded neighbor  $a_1'$ .

#### Alignment to preserve the core bonding direction

For each core connection site  $a_0$ , the substituent fragment is rigidly aligned such that the fragment is placed along the original bond direction in the core. The alignment enforces linear geometries

$$\angle a_0' - a_0 - a_1 = 180^\circ \quad \text{and} \quad \angle a_0 - a_1 - a_1' = 180^\circ,$$

so that the substituent is oriented “straight out” from the core along the  $a_0' - a_0$  direction.

### Translation to set the target bond length

After angular alignment, the substituent fragment is translated along the attachment axis without additional rotation. The translation distance is chosen such that

$$d(a'_0, a'_1) = [r(a'_0) + r(a'_1)] \times s,$$

where  $r$  is the covalent radius and  $s$  is a `scaling_factor` parameter (default:  $s = 1.0$ ).

### Bond formation via terminal-atom deletion and index retention

Finally, the terminal atoms  $a_0$  (in the core) and  $a_1$  (in the substituent) are removed, which results in the formation of a new covalent bond between  $a'_0$  and  $a'_1$  at the attachment site. To enable robust handling of multiple substitution sites specified by the core connection index list, the atom index of  $a'_1$  in the merged structure is reassigned to  $a_0$  (i.e., the original terminal atom index in the core). With this convention, the connection site indices remain consistent throughout successive substitutions, thereby preventing index-shift issues during multi-site structure modification.

### Post-attachment sanitization by rotational adjustment.

For all structure editing tools, a geometry sanitization procedure is applied to eliminate unphysical atomic overlaps between the core structure and newly attached fragments. After fragment attachment, interatomic distances are evaluated between atoms in the core structure and atoms in the newly added fragment. Let  $i$  denote an atom index in the core structure and  $j$  an atom index in the attached fragment. A steric clash is defined when the distance  $d(i, j)$  satisfies

$$d(i, j) < 1.4 \times [r(i) + r(j)],$$

where  $r(i)$  and  $r(j)$  are the covalent radii of atoms  $i$  and  $j$ , respectively.

If any such clashes are detected, the attached fragment is iteratively rotated about the newly formed bond in increments of  $5^\circ$ . After each rotation, the interatomic distances are re-evaluated until all  $d(i, j)$  exceed the threshold defined above. This procedure preserves the internal geometry of both the core structure and the fragment while ensuring a sterically reasonable initial configuration for subsequent calculations.

### Predefined fragments

For commonly used substituents, we provide a predefined fragment library ([Figure S6](#)). For fragments in this library, the terminal attachment atom and its bonded neighbor are predefined, with  $a_1$  and  $a'_1$  fixed to indices 0 and 1, respectively. As a result, when a predefined fragment is used, it is not necessary to generate a separate substituent-specific `xyz` file. Instead, the agent can simply specify the fragment name.

In this case, both `FG_connection_idx` and `binding_mode` are implicitly defined by the fragment template and therefore do not need to be provided.

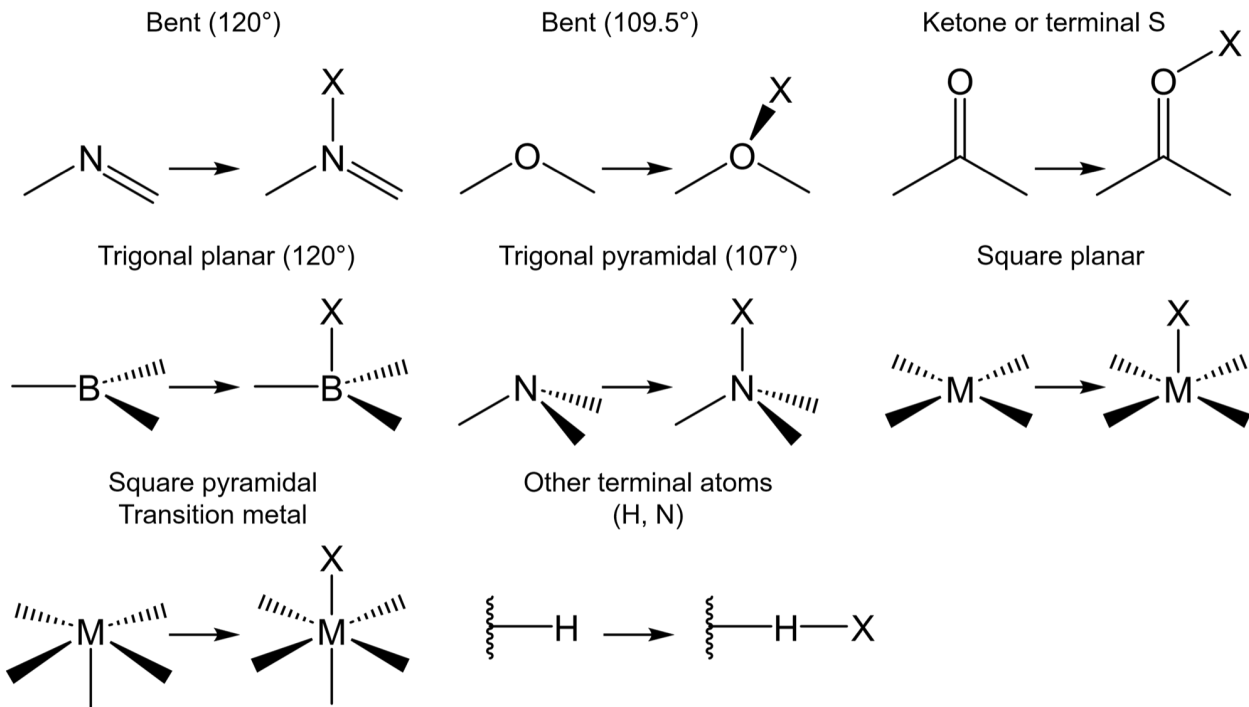


**Figure S4** VSEPR-guided placement of new bonds in the binding tool. A dummy atom (X) is introduced to indicate the direction of the newly created bond, with its position determined according to VSEPR-based idealized geometries for different central atoms and coordination environments.

To determine the appropriate placement of dummy atoms for fragment binding, the local coordination geometry around the central atom is first analysed and compared against a set of predefined ideal VSEPR geometries. For each candidate VSEPR geometry with a given coordination number, the angles between neighbouring atoms are computed and compared to the corresponding set of ideal angles.

A similarity score is assigned to each candidate geometry based on the deviation between observed angles and ideal VSEPR angles. Let  $\{\theta_k\}$  denote the set of observed angles and  $\{\theta_k^{\text{ideal}}\}$  the corresponding ideal angles. For each geometry, a score is computed as

$$\text{score} = \frac{1}{N} \sum_k \exp \left( -\frac{(\theta_k - \theta_k^{\text{ideal}})^2}{2\sigma^2} \right),$$

where  $N$  is the number of angles considered and  $\sigma$  is a smoothing parameter controlling angular tolerance. In this work,  $\sigma$  is set to 5.7°.

The coordination geometry corresponding to the highest score is selected, provided that the score exceeds a threshold value of 0.6. If this criterion is satisfied, dummy atoms are placed at the missing coordination positions defined by the selected ideal VSEPR geometry, using a fixed bond length (1.0 Å).

If no candidate VSEPR geometry satisfies the scoring threshold, a fallback procedure is employed. In this case, a grid-based angular search is performed around the central atom to identify sterically accessible directions with minimal overlap with existing atoms. A dummy atom is then placed in the least sterically hindered direction at a fixed distance of 1.0 Å from the central atom. This strategy ensures robust dummy atom placement even for irregular or highly distorted coordination environments.

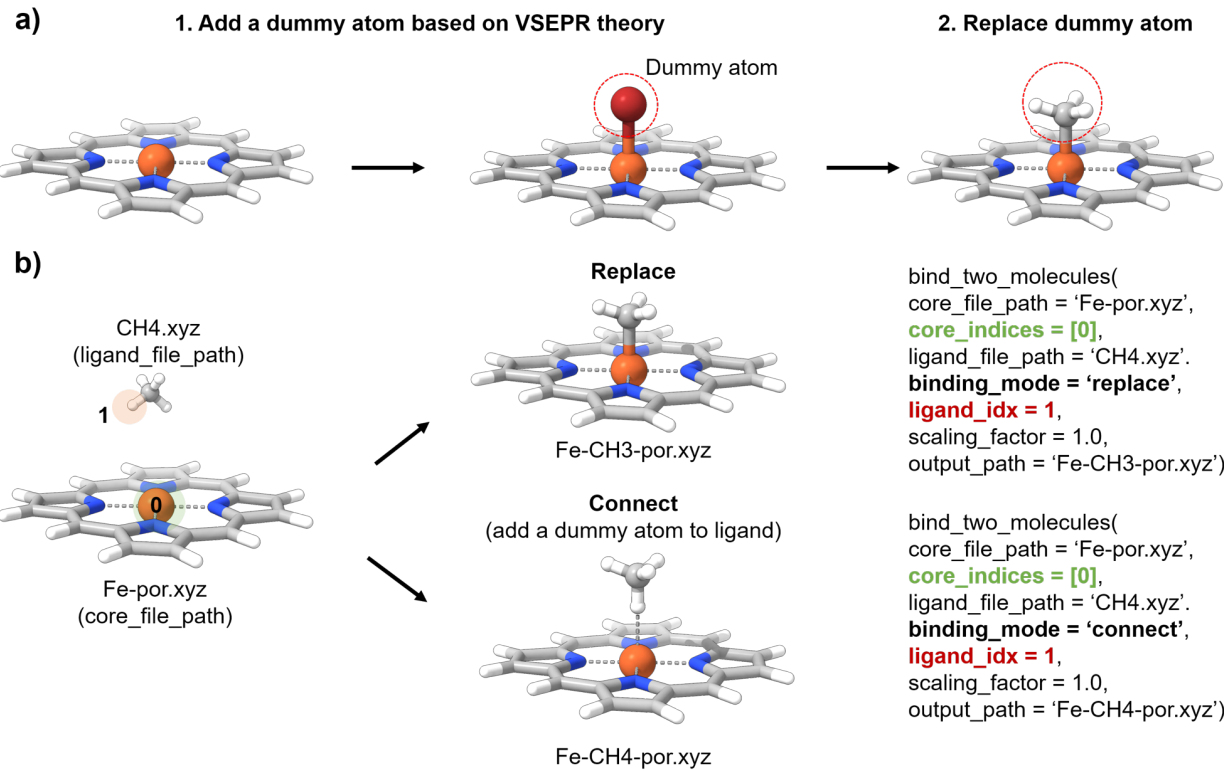


**Figure S5** Detailed mechanism and arguments of bind\_two\_molecules tool. (a) Schematic workflow of the binding tool. The initial molecular structure, the applied replacement with its input parameters, and the resulting structure after the operation for (b) binding\_mode = 'replace', (c) binding\_mode = 'connect'. Atom color codes: dark orange, Fe; blue, N; gray, C; white, H.

**Binding tool via dummy-atom introduction** The binding tool operates by first introducing a dummy atom at specified indices in the core structure, according to the local VSEPR geometry (Figure S4). Once added, this dummy atom is treated as a terminal atom and serves as the attachment site for subsequent fragment binding.

After the dummy atom is introduced, the binding procedure follows the same workflow as the replace\_terminal\_atoms\_with\_fragment tool (Figure S3). Specifically, fragment alignment, bond-length setting, binding mode (replace or connect), and using predefined fragments are applied in an identical manner. As a result, the binding tool can be viewed as a two-step process: (i) generation of a terminal attachment site via a dummy atom, followed by (ii) standard fragment replacement or connection.

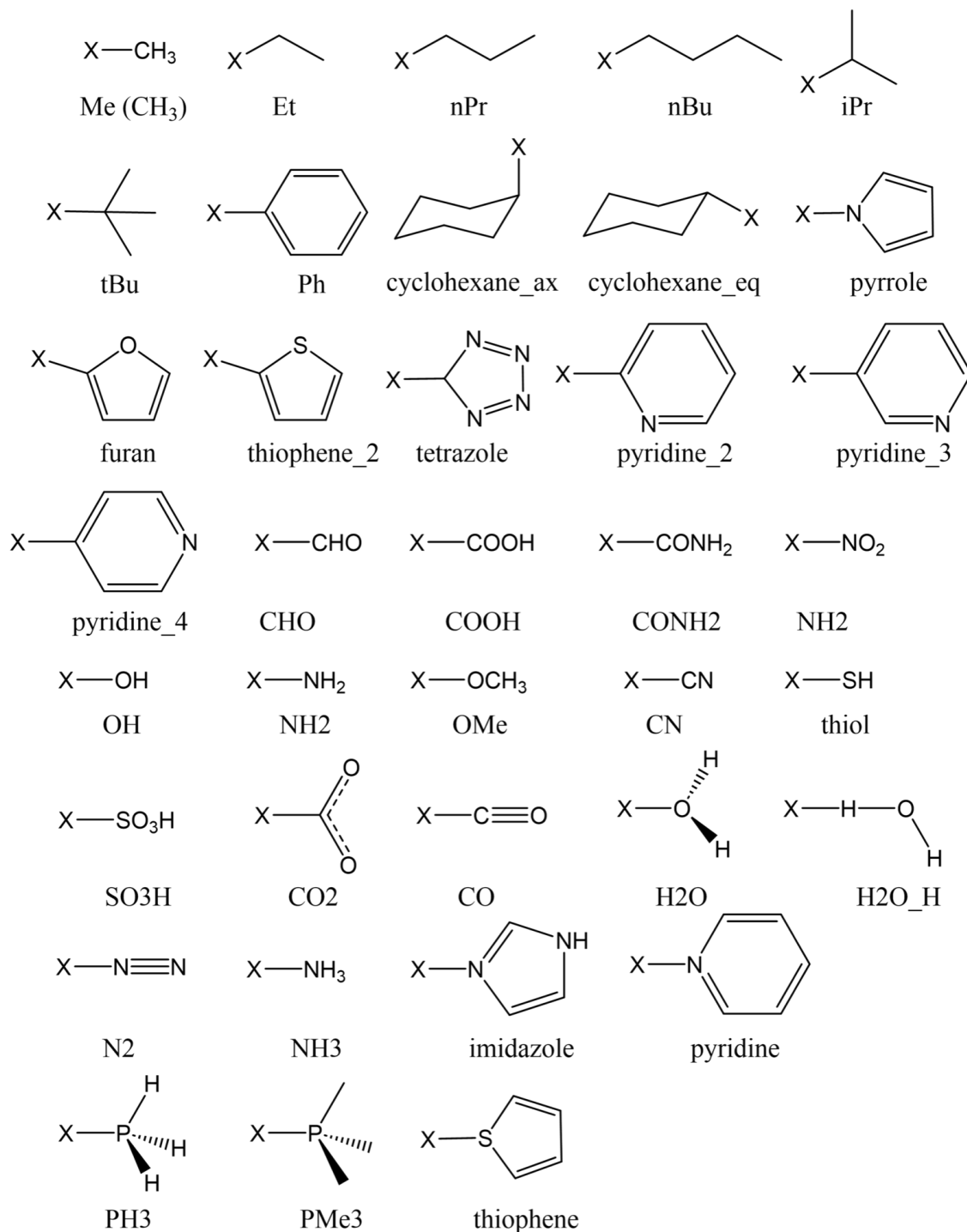


**Figure S6** Predefined fragment library used for replacement and binding operations. Labels shown below each structure correspond to the fragment names as stored in the library. X denotes the connection site.

## B.4 Structure Generation Tools

### Transition-metal complex construction from coordination templates.

The transition-metal complex construction tool builds metal-ligand structures starting from a predefined coordination-geometry template. In all templates, the central metal atom is fixed to atom index 0. A library of predefined coordination geometries (e.g., square planar, octahedral, tetrahedral) is provided, and the desired geometry is selected via the `coordination_geometry` argument.

By default, all coordination sites in the selected template are occupied by monodentate placeholder ligands (Cl atoms). Therefore, explicitly specifying monodentate ligands such as Cl is optional. When a metal element is provided via the `metal` argument, the element at atom index 0 is reassigned accordingly.

### Ligand binding specification and polydentate attachment.

Ligand attachment is controlled by the `ligand_bindings` argument, which is provided as a list of dictionaries mapping ligand names to coordination site indices. For polydentate ligands, multiple coordination indices must be specified simultaneously. For example, a bidentate ligand such as 1,10-phenanthroline (phen) is attached by specifying two coordination indices (e.g., [1,2]), which are treated as a single binding event.

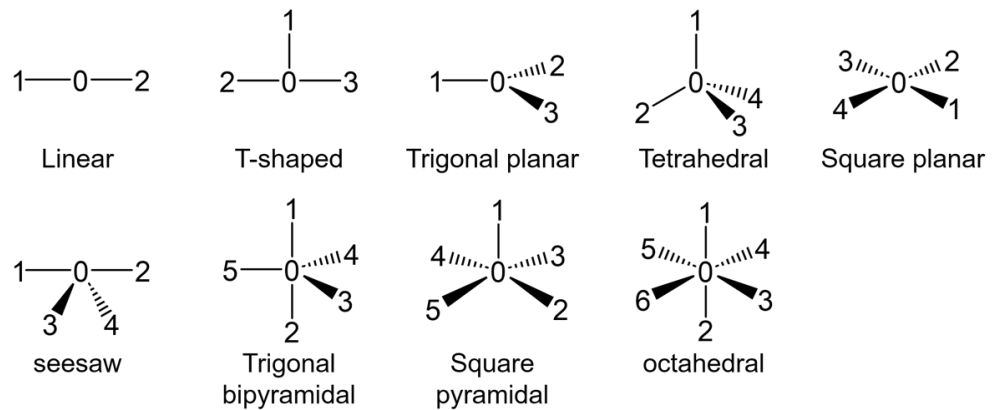
A predefined library of common polydentate ligands is provided ([Figure S8](#)). These ligands are stored with preassigned dummy atoms that encode their preferred binding geometry. During attachment, the ligand is aligned to the coordination template according to the mechanism illustrated in the figure, ensuring consistent chelation geometry.

For polydentate ligands, attachment proceeds according to the predefined alignment mechanism shown in the [Figure S7](#), using the dummy atoms embedded in the ligand template. In contrast, for standard monodentate substitutions not covered by the polydentate library, ligand attachment is performed in the same manner as the general atom-replacement workflow, following the procedures described for the `replace` tool.

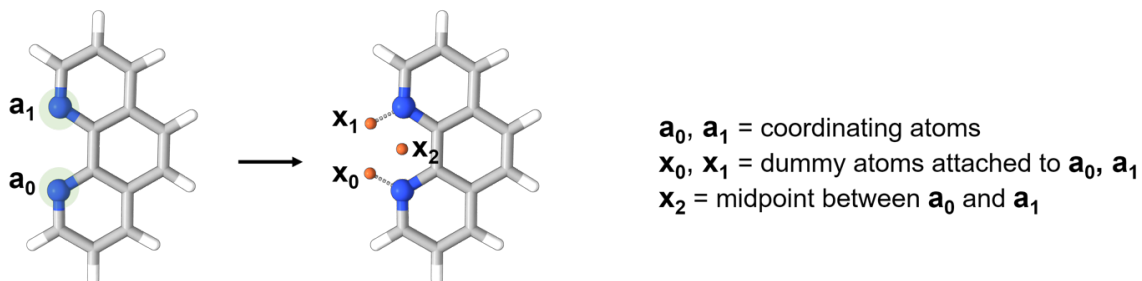
The structure shown in [Figure S7](#) was generated using the following tool invocation:

```
build_tm_complex_from_template(  
    coordination_geometry = 'square_planar',  
    metal = 'Pd',  
    ligand_bindings = [{  
        'phen': [1,2]  
    }],  
    output_path = 'Pd_phen_Cl2.xyz'  
)
```

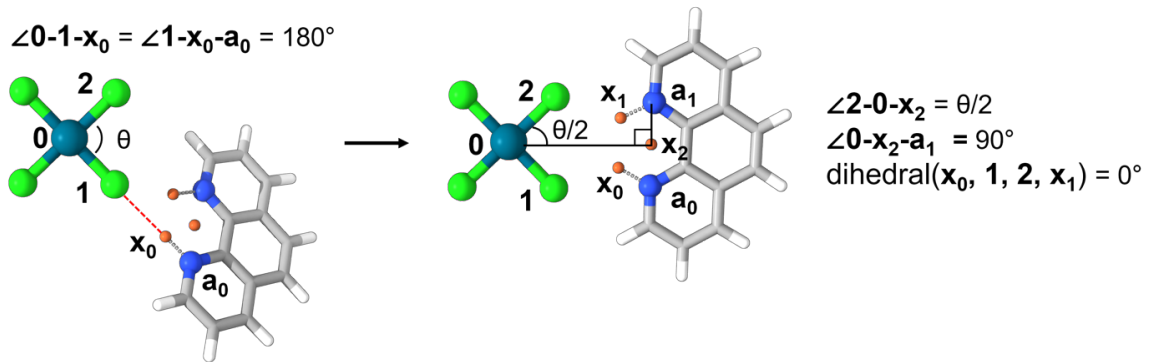
## 1. Library of predefined coordination geometries with atomic indices



## 2. Insertion of dummy atoms at coordinating sites



### 3. Ligand alignment along the connection direction



#### 4. Fragment merging by controlled reduction of the $0-x_2$ distance

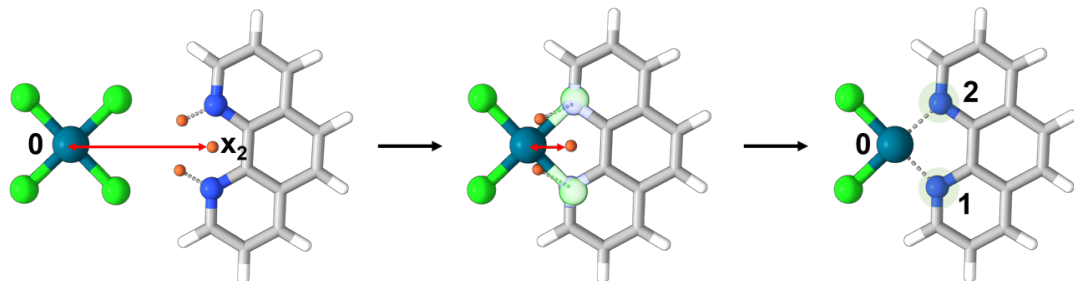


**Figure S7** Detailed mechanism and arguments of the organometallic structures builder. Atom color codes: green, Pd; lime green, Cl; blue, N; gray, C; white, H, dummy atom; orange.

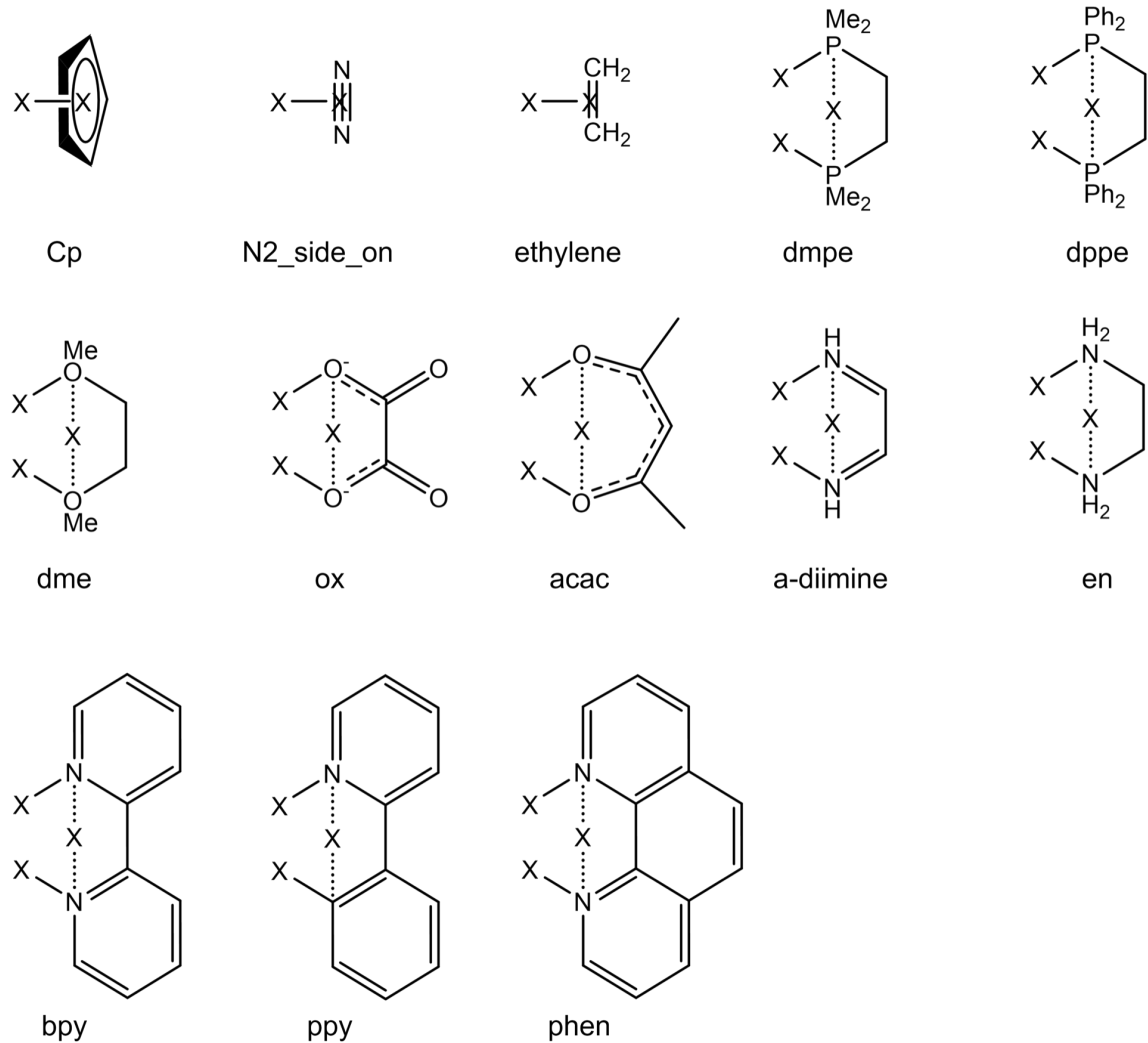


**Figure S8** Predefined polydentate ligands library used for replacement and binding operations. Labels shown below each structure correspond to the fragment names as stored in the library. X denotes the connection site.

## C VLM benchmark system prompt

In this section, we list the VLM benchmark system prompt for all five Vision-Language Models (Gemini 3 Pro, Gemini 3 Flash, Sonnet 4.5, Opus 4.5, and GPT 5.2), and list an example for the use of `view_molecule` and `zoom_molecule` tool in the benchmark. .

### System Prompt

You're a helpful scientific agent. Here is Your Current Role: you are a helpful chemistry vision agent. You will be tasked to identify correct neighbour atoms. You should use vision capability only, which you can view the molecule by using the given tools. You can rotate the molecule to inspect it in different angles. You can also zoom in to get a better view especially when view is too crowded. Do not overthink, this is a simple vision task.

### Tool Used for geomconf\_1027

Following pictures show the example of geomconf\_1027 using `view_molecule_tool` and `zoom_molecule_tool` to zoom the target region, in order to gain a better vision information.

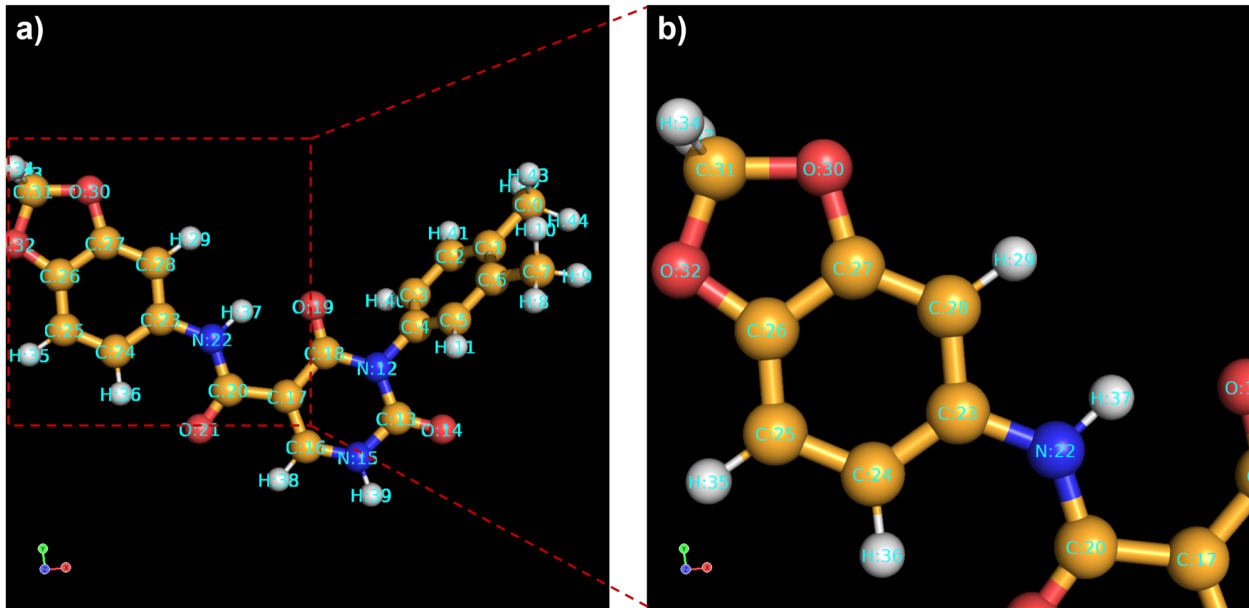


**Figure S9** (a) Visualization using the `view_xyz_tool`. The tool displays the full molecule (global view) by resetting previous zoom levels. (b) Zoomed-in view of the molecular structure. This perspective allows for a detailed inspection of local atomic environments.

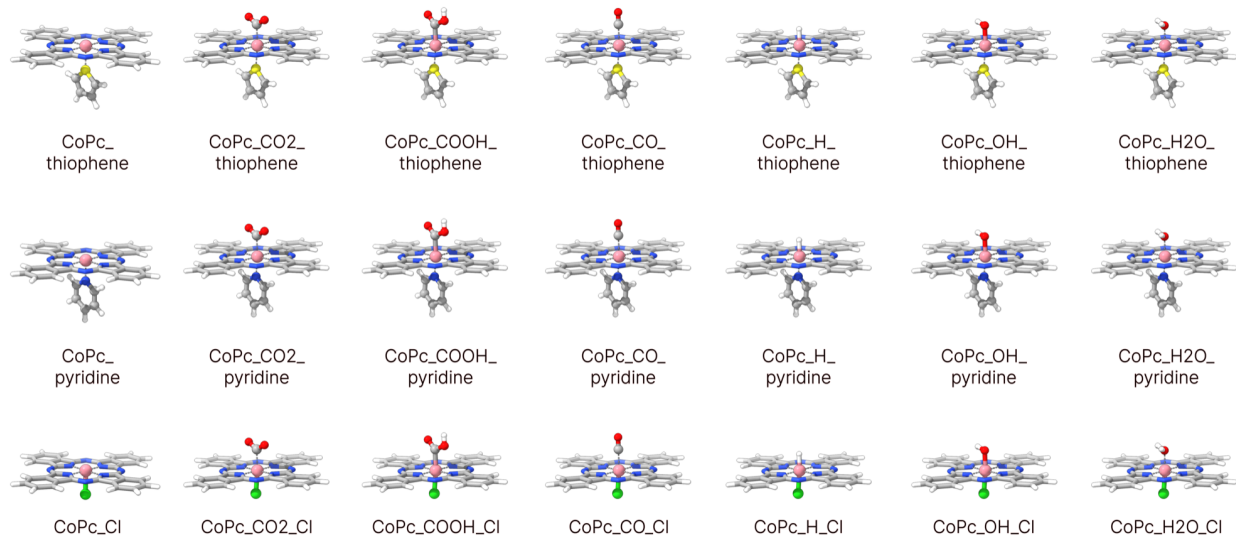


**Figure S10** Full list of Co-phthalocyanine (CoPc) complexes generated by the agent with different axial ligands (thiophene, pyridine, and Cl). The structure labels shown below each complex correspond to the filenames used by the agent during structure generation, while the .xyz extension is omitted for clarity. The Co center, together with the bound intermediates (CO<sub>2</sub>, COOH, CO, H, OH, and H<sub>2</sub>O), and axial ligands (thiophene, pyridine, or Cl) are highlighted using a ball-and-stick representation, while the remaining atoms are rendered as sticks for clarity. Atom color codes: pink, Co; lime green, Cl; yellow, sulfur; red, O; blue, N; gray, C; white, H.

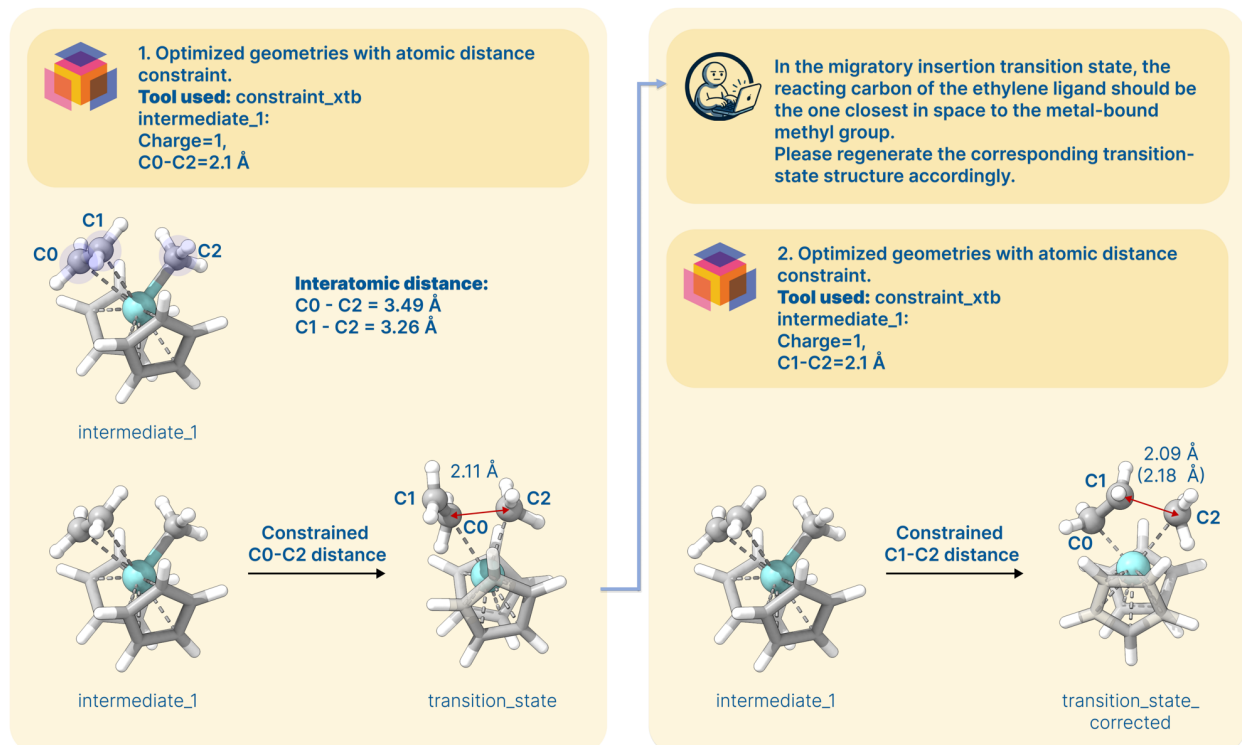


**Figure S11** An unwanted structure obtained when an arbitrary carbon atom of the ethylene ligand was selected for constraint application (left) and a chemically reasonable transition-state structure obtained after selecting the ethylene carbon atom closest to the metal-bound methyl group through the second prompt.